

# **DISCRETE AND CONTINUOUS ONE-DIMENSIONAL MODELS OF PARASYSTOLE**

Khady Diagne

Department of Physiology  
McGill University

Montreal, Canada  
August 2020

A thesis submitted to the Faculty of Graduate Studies and Research in partial fulfillment of the requirements for the degree of Master of Science

© **Khady Diagne, 2020**

## TABLE OF CONTENTS

ABSTRACT .....	3
RÉSUMÉ .....	4
ACKNOWLEDGEMENTS .....	5
CONTRIBUTION OF AUTHORS .....	6
CHAPTER I: INTRODUCTION AND REVIEW OF LITERATURE .....	7
1.1: Normal Cardiac Rhythm .....	7
1.1.1: Cardiac Electrophysiology .....	7
1.1.2: The Cardiac Rhythm .....	9
1.2: Arrhythmias .....	11
1.2.1: The Electrocardiogram (ECG) .....	11
1.2.2: Defining Arrhythmias .....	13
1.2.3: Premature beats .....	15
1.3: Parasystole .....	16
1.3.1: History .....	16
1.3.2: Experimental Models .....	18
1.3.3: Mathematical models .....	21
1.4: Rationale and goal .....	26
CHAPTER 2: CELLULAR AUTOMATON MODEL .....	28
2.1: Methods .....	28
2.2: Results .....	29
2.2.1: Characteristics of model .....	29
2.2.2: NIB evolution in space .....	31
2.2.3: NIB vs $T_{EP}/T_{SN}$ .....	36
2.2.4: Comparing to real recordings .....	37
CHAPTER 3: FITZHUGH-NAGUMO DIFFERENTIAL EQUATIONS MODEL .....	39
3.1: Methods .....	39
3.2: Results .....	41
CHAPTER 4: DISCUSSION .....	49
4.1: Limitations .....	49
4.2: Conclusions .....	49
4.3: Future directions .....	51
REFERENCES .....	55

## ABSTRACT

In the healthy heart, the sinoatrial node is the only pacemaking region and thus initiates depolarization waves that result in cardiac contractions. However, in diseased tissue, a second pacemaker can arise in either the atria or the ventricles. Activation of this ectopic focus causes premature ventricular or atrial complexes and this phenomenon, called parasystole, results in an irregular rhythm. Two types of parasystole have been identified: modulated parasystole, where the pacemakers can electronically influence each other and pure parasystole, where the two pacemakers are protected from each other. In previous theoretical models, the interaction of two pacemakers is simulated without considering physical space and the distance between them. In real tissue, the two pacemakers are embedded in an excitable medium that supports electrical impulses. The goal of this project is to build simple theoretical models of pure parasystole that include the spatial component in order to allow us to observe activation patterns in space. I built two models of parasystole that include space. In the first, I simulate the dynamics using a cellular automaton, that is discrete in time and in space and allows a direct mapping of key physiological parameters to user defined variables. The second model is based on the Fitzhugh-Nagumo dynamical equations. In this continuous model of excitable media, cells can either be stimulated at a fixed rate or parameters can be adjusted so that they intrinsically fire. Results from our simulations from both models suggest that the evolution of dynamical patterns in space matches that seen in models without a spatial component as the refractory period is increased. These models of pure parasystole provided insight in the physical dynamics of parasystole and will be used to further study pure and modulated parasystole.

*Keywords:* Premature ventricular complexes, Parasystole, Cellular Automaton, Fitzhugh-Nagumo.

## RÉSUMÉ

Dans le cœur sain, le nœud sino-auriculaire commande le rythme et les contractions cardiaques et est ainsi le seul stimulateur cardiaque. Or, dans les tissus malades, un deuxième stimulateur cardiaque peut apparaître dans les oreillettes ou les ventricules. L'activation de ce foyer ectopique provoque des complexes ventriculaires ou auriculaires prématurés et ce phénomène, appelé parasystole, se traduit par un rythme irrégulier. Deux types de parasystole ont été identifiés : la parasystole modulée, où les stimulateurs cardiaques peuvent s'influencer électroniquement et la parasystole pure, où les deux stimulateurs cardiaques sont protégés l'un de l'autre. Dans tous les modèles théoriques publiés, l'interaction de deux stimulateurs cardiaques est simulée sans tenir compte de l'espace physique et de la distance qui les sépare. Cependant, dans le cœur, les deux stimulateurs cardiaques sont intégrés dans un milieu excitable qui supporte les impulsions électriques. Le but de ce projet est de construire des modèles théoriques de parasystole qui incluent la dimension spatiale afin de nous permettre d'observer des modèles d'activation dans l'espace. Nous avons construit deux modèles de parasystole qui incluent l'espace. Dans le premier, nous simulons la dynamique à l'aide d'un automate cellulaire, qui est discret dans le temps et dans l'espace et permet une cartographie directe des paramètres physiologiques clés aux variables définies par l'utilisateur. Le deuxième modèle est basé sur les équations dynamiques de Fitzhugh-Nagumo. Dans ce modèle continu de milieux tissu excitable, les stimulateurs cardiaques peuvent être stimulés à un rythme fixe ou les paramètres peuvent être ajustés de manière à ce qu'ils s'activent intrinsèquement. Les résultats de nos simulations des deux modèles suggèrent que l'évolution des dynamiques dans l'espace correspond à celle observée dans les modèles sans composante spatiale lorsque la période réfractaire est augmentée. Ces modèles de parasystole pure ont fourni un aperçu de la dynamique spatiale de parasystole et seront utilisés pour étudier en profondeur la parasystole.

*Mots-clés* : Complexes ventriculaires prématurés, Parasystole, Automate cellulaire, Fitzhugh-Nagumo

## ACKNOWLEDGEMENTS

I would like to extend my gratitude first and foremost to my professors Dr. Gil Bub and Dr. Leon Glass for all the help, guidance and advice they've provided throughout my entire Master's program and without whom this project could not take place.

I would also like to thank lab members Miguel Romero Sepúlveda who trained me in making cardiomyocyte monolayers and Tom Bury who helped me navigate through the software program Python and has analyzed Holter recordings from patients.

My supervisory committee: Dr. Michael Guevara, Dr. Alvin Shrier and Dr. Arjun Krishnaswamy who have provided useful insights and suggestions.

A special thanks to Ms. Rosie Vasile, the administrative student affairs coordinator for graduate studies from the Department of Physiology for she has helped me, time and time again, navigate through the administrative requirements of the program allowing me to fully focus on my project.

Last, but certainly not least, I would like to thank my family and friends – especially my brother and my parents– for the unconditional love, support and encouragement.

## CONTRIBUTION OF AUTHORS

Tom Bury analyzed Holter recordings data and built Fig. 12 from this. Miguel Romero Sepúlveda made the cardiomyocyte monolayer mentioned in the discussion and Dr. Gil Bub stimulated and recorded this monolayer.

All other experiments and simulations and the thesis writing were done by me, under the supervision and guidance of Dr. Gil Bub and Dr. Leon Glass.

## CHAPTER I: INTRODUCTION AND REVIEW OF LITERATURE

### 1.1: Normal Cardiac Rhythm

#### 1.1.1: Cardiac Electrophysiology

In all mammals, the heart is functionally and structurally separated into the left and right sides. The right side of the heart takes deoxygenated blood from the body and sends it to the lungs, whereas the left side of the heart takes oxygenated blood from the lungs and sends it back to the body. Each side of the heart is further divided into upper and lower chambers: the atria and the ventricles. The atria sit at the top: the right atrium receives blood from the venae cavae and the left atrium receives blood from the pulmonary veins. Blood then flows to the right and left ventricles, which expel blood out of the heart through the pulmonary arteries and the aorta, respectively (Anderson et al., 2004).

The heart's function depends on its ability to propagate action potentials and contract in synchrony. An action potential (AP) is defined as a brief electrical depolarization and repolarization near the cellular membrane (Kléber & Rudy, 2004). In muscle cells, the AP leads to muscle contraction. The resting potential of a cell is usually around  $-70\text{mV}$  (although it can range from  $-90\text{mV}$  to  $-50\text{mV}$ ). The AP is initiated when the membrane potential of a cell is depolarized to a threshold value. Once this value is reached, voltage-gated sodium channels begin to open and the rapid influx of  $\text{Na}^+$  ions cause the rapid upstroke of the AP. However, the channels quickly inactivate, and the cell begins to repolarize. At this time, voltage-gated potassium channels are opening, and this will cause a hyperpolarization of the membrane at which point the voltage-gated potassium channels close and the cell can regain its resting state (Bean et al., 2007).

In the healthy heart, the action potential originates from the sinoatrial (SA) node that sits in the top right of the right atria. In cardiomyocytes the membrane resting potential is at about  $-90\text{mV}$ , in the SA node however, the resting potential fluctuates and is subject to a slow and steady depolarization. This is the pacemaker current and it is due to a hyperpolarization-activated channel (Verkerk et al., 2007). This eventually brings the membrane potential to threshold, which is about

-35mV, and the AP is triggered. The depolarization at the SA node propagates to the right and left atria through gap junctions that connect the cardiomyocytes. The propagating AP is slowed at the atrioventricular (AV) node, situated at the base of the right atria near the interatrial septum. This gives time to both atria to completely depolarize and contract at the same time before the ventricles (Kléber & Rudy, 2004). The AP then leaves the AV node through the bundle of His into the interventricular septum. The bundle of His is a pathway of specialized cardiomyocytes that can quickly propagate the AP throughout the ventricles. It separates into left and right branches, termed Purkinje fibers, that form a network to innervate and depolarize the left and right ventricles respectively (Alanís et al., 1958). The branched network of Purkinje fibers within the ventricles allows for the synchronous depolarization of the ventricles. Once the AP reaches a cardiomyocyte in the ventricles or the atria, excluding the SA node, the voltage gated sodium channels quickly open as above mentioned. This depolarization causes the opening of the voltage-gated calcium channels, these slow channels remain open even after the voltage-gated sodium channels inactivate. Particular to cardiomyocytes however, the voltage-gated calcium channels remain open for a long time, causing the long plateau phase. This influx of  $\text{Ca}^{2+}$  ions maintains the membrane potential at a plateau at 0mV for about 250msec after which the voltage-gated calcium channels close and the voltage-gated potassium channels open and repolarize the cell membrane (Kléber & Rudy, 2004).

The excitation-contraction coupling mechanism allows for the propagated AP to trigger muscle contraction in the whole heart. The coupling between the electrical impulse and physical contraction is mediated by  $\text{Ca}^{2+}$  ions. During the plateau phase of the action potential, voltage-gated calcium channels in the T tubules open and allow for an influx of  $\text{Ca}^{2+}$  ions from the extracellular space. These ions can then bind the ligand-gated calcium channels at the surface of the sarcoplasmic reticulum. This results in a large migration of  $\text{Ca}^{2+}$  ions from the sarcoplasmic reticulum into the cytosol. This calcium-induced calcium release, as in skeletal muscle, increases cytosolic calcium concentration and allows for  $\text{Ca}^{2+}$  ions to bind troponin and expose the myosin binding sites on the actin filament. Cross-bridge formation between the myosin and the actin can then occur, which results in the physical shortening of the cell at the small scale and muscle contraction at the large scale (Bers et al., 2002). Through this coupling mechanism, the heart can depolarize and contract in a rhythmic fashion.

### 1.1.2: The Cardiac Rhythm

Without neural input, the SA node has an intrinsic rate of about 100 beats/min. The autonomous nervous system (ANS) controls the heart rate through the parasympathetic and sympathetic systems (Dampney et al., 1994).

On one hand, the parasympathetic branch, responsible for “rest and digest” type responses, acts on the heart via the vagus nerve. The vagus nerve is a parasympathetic preganglionic nerve that releases acetylcholine (ACh) to postganglionic nerves in the cardiac ganglia. In turn, these postganglionic nerves also release ACh, which binds G-coupled muscarinic receptors. Muscarinic receptors are principally in the SA node, the AV node and the atrial tissue but are sparse in the ventricles. When ACh binds muscarinic receptors, it triggers a cascade of events in cardiomyocytes that overall result in the decrease of cardiac output (CO). In the SA node, their activation hyperpolarizes the cells and decreases the slope of depolarization, making it longer to reach threshold and thus reducing heart rate (HR). In the AV node, when activated, these receptors reduce the conduction velocity, slowing down even further AP propagation to the ventricles. Finally, in atrial cardiomyocytes, they reduce contractility which decreases stroke volume (SV). From Fick’s law:  $CO = SV \times HR$ , decreasing SV and/or HR will directly decrease CO.

On the other hand, postganglionic nerves from the sympathetic ganglia chain release norepinephrine (NE) to adrenergic receptors of the heart. Activation of the  $\beta_1$ -adrenergic receptors, also G-coupled receptors, increases heart rate in the SA node, conduction velocity in the AV node and contractility in the other cardiomyocytes (both atria and ventricles). The sympathetic branch then yields the opposite effect of the vagus nerve by decreasing HR and SV to decrease CO.

Thus, depending on the physiological demands of the body, the ANS can finely and quickly tune the heart rate, along with blood pressure and cardiac output. However, other organs can release hormones in the bloodstream that will modulate cardiac functions. For instance, the adrenal medulla releases epinephrine when the blood pressure is low. However, most hormones released by the kidneys or posterior pituitary gland directly act on vasculature to promote either vasodilation or vasoconstriction (Gordan et al., 2015).

The normal resting heart rate is of about 70 beats/min and this can fluctuate depending on age and gender. This value suggests that there is an almost constant vagal tone on the heart to prevent it from beating at its own, faster pace. Note however that even though the mean HR is constant, small beat-to-beat variations in cycle lengths can be observed in all healthy humans. This is referred to as Heart Rate Variability (HRV). HRV is a physiological and normal phenomenon that is dependent on many factors including gender, age, respiration, orthostasis (fall in BP when standing), sleep-wake cycle and cardiovascular conditioning (Acharya et al., 2006). Beat-to-beat variations in ionic concentration near the SA node can result in HRV. In addition, recall that the SA node is controlled by vagal and sympathetic tone, and so, variations in their activity can also affect cardiac rhythm. Studies in the last decades have isolated some important characteristics of HRV. HRV can be classified into four categories: high frequency, low frequency, very low frequency and ultra-low frequency (Malik et al., 1996). The high frequency HRV is due to respiratory sinus arrhythmia. As atrial pressure decreases during inhalation, there is an increased blood flow to the region which triggers baroreceptors. This causes the ANS to increase vagal tone and to reduce blood pressure and heart rate (Médigue et al., 2001). The low frequency HRV are associated with the sympathetic nerve. The very low and ultra-low frequency HRV are caused by less recurring events of longer period such as circadian rhythms (Malik et al., 1996). This is to say that healthy HR is not and should not remain constant even when the mean HR is.

Alternans is another type of beat-to-beat variations, however unlike HRV, alternans is often associated to cardiac pathology. Alternans is defined as regular beat to beat variations in the strength of contraction (mechanical alternans) or in the AP shape (electrical alternans) (Euler, 1999) and have been shown to be obtained during fast pacing of mammalian hearts (Guevara et al., 1989). One of the proposed mechanisms of mechanical alternans is based on the Frank-Starling relationship. This suggests that a weak contraction leaves a larger end-diastolic volume which results in a stronger contraction that in turn leaves a smaller end-diastolic volume. This then causes the next beat to be weaker and the cycle continues. This process is more pronounced at higher pacing frequencies since there will be less time allowed for diastolic filling (Euler, 1999). Another possible reasons for mechanical alternans is that there are two subpopulations of cells that are alternatively beating (Guevara et al., 1989). Electrical alternans however are believed to be mainly

due to mechanical alternans: the alternation in sarcoplasmic reticulum-released  $\text{Ca}^{2+}$  ions due to alternating forces of contraction influences the action potential durations. The presence of alternans have been correlated to a greater incidence of cardiac disease (Euler, 1999) and associated to re-entry and cardiac arrhythmias (Weiss et al., 2011).

## **1.2: Arrhythmias**

### **1.2.1: The Electrocardiogram (ECG)**

The most efficient and least invasive method of assessing cardiac function is the electrocardiograph. The electrocardiograph is a tool that has originated in the late 19<sup>th</sup> century. Many scientists have worked on improving its function and accessibility. The first human electrocardiogram (ECG), which is in fact a polygraphic curve, was recorded, using electrodes and a capillary electrometer, in 1887 by British physiologist Augustus Waller (Waller, 1886). The capillary electrometer measures small electric pulses by detecting changes in the surface tension between mercury and sulfuric acid within an asymmetrical tube (the sulfuric acid being in the thinner end) (Lucas, 1912). Following the works of Waller, Dutch physiologist Willem Einthoven improved the capillary electrometer and mathematically corrected the tracings to account for inertia in the system. The initial waves were labelled ABCD and Einthoven labelled his corrected curves PQRST (Fig. 1). This PQRST curve represents observable electrical activity of the heart at the surface of the skin during a contraction and corresponds to the same ECG curve we would expect today. The P-wave represents the atrial depolarization. About 150msec later is the QRS complex which represents the ventricles depolarization. And lastly, the T-wave is the ventricular repolarization. Atrial repolarization is not visible in the ECG as it occurs during the ventricle depolarization. (AlGhatrif & Lindsay, 2012). Note however that the ECG is a measurement of changes in extracellular electrical activity, as a result of the synchronized changes occurring in the cardiomyocytes. Thus, whereas depolarization in a single cardiac cell takes about 5 to 10 ms, the overall recorded QRS complex lasts about 100msec.

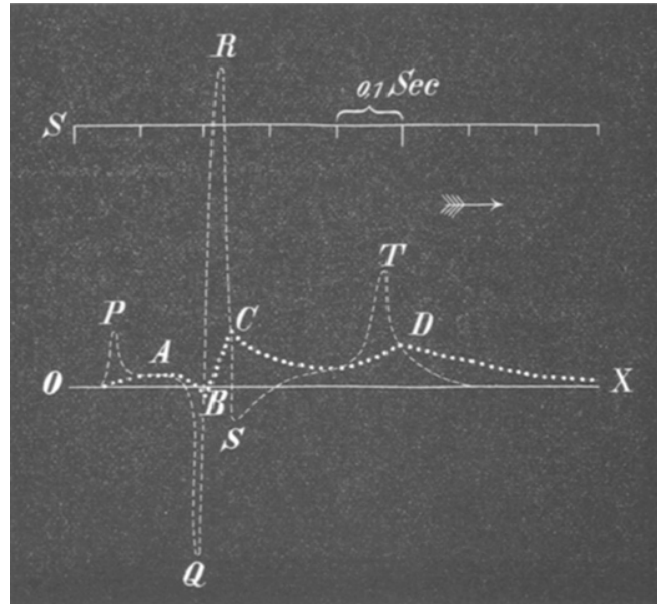


**Figure 1:** The uncorrected (ABCD) and Einthoven's corrected (PQRST) ECG curves (from AlGhatrif & Lindsay 2012)

Einthoven coined the term electrocardiogram to refer to these waveforms in 1893. In 1924, he was awarded the Nobel Prize of Physiology and Medicine for his invention of the electrocardiograph. In the following decades, improvements to the electrocardiograph have made it more accurate, but also smaller and portable. In Waller's model, 5 electrodes were placed on the patient: one on each arm and leg and one in the mouth. Einthoven's model only required electrodes at both arms (RA and LA) and on the left leg (LL) as he had concluded they gave the greatest yield. Measurements were made by comparing potentials at two different surfaces of the body; one electrode defined to be the negative pole and the other the positive pole. The voltage difference between the two electrodes, going from negative to positive, is referred to as a lead. And so, from the three electrodes, Einthoven defined three leads. Lead I is the difference from LA to RA, lead II is the difference from LL to RA and lead III is the difference from LL to RA. These three leads are called Einthoven's triangle, which is still at the basis of the electrocardiograph today. However, this was not enough: the three leads – three point-of-views – only gave a limited vision of the heart and more leads would be required to have a more complete perspective. In 1934, Dr. Frank Wilson developed a unipolar lead that could be used to 'explore' potential differences at any point on the body. This was done by using the average of the three previously described leads as a ground electrode and placing another electrode at any desired position. This method gave rise to the

precordial leads: six more electrodes labelled V1 to V6 were placed on the precordium horizontally spanning the heart. Whereas the limb leads were bipolar (potential difference at two points in space), the precordial leads are unipolar. In 1942, Dr. Emmanuel Goldberger created augmented unipolar limb leads, based on Wilson's methods. For instance, at the RA, the augmented unipolar lead (a-VR) is the difference between the potential at the RA and the average at two other points, LA and LL. Similarly, the augmented unipolar limb leads at LA and LL are labelled a-VL and a-VF respectively (AlGhatrif & Lindsay, 2012). Limb leads I through III, precordium leads V1 to V6 and augmented leads a-VR, a-VL and a-VF represent the 12 possible leads as seen in modern electrocardiographs.

### 1.2.2: Defining Arrhythmias

The initial purpose of the ECG, since its first development in the 20<sup>th</sup> century, was to study arrhythmias which are irregular or abnormal cardiac rhythms. During the first half of the 20<sup>th</sup> century, an increasing number of experiments have been conducted to analyse these rhythms. Thus, the electrocardiograph was the precursor to cardiac electrophysiology which has greatly increased our knowledge of cardiac function and cardiac disease. As the cardiac electrical-mechanical coupling activity is complex, there are many steps within cardiac depolarization and/or contraction that can affect normal cardiac function if impaired. This results in a panoply of different arrhythmias that can be classified by symptoms, rate, duration or mechanism. Arrhythmic symptoms can range from none to shortness of breath, chest pain or even death if left untreated. As for the rate, fast heart rates are named tachycardias (over 100 bpm) and slow heart rates are bradycardias (under 60 bpm). Next, some arrhythmias can be short in duration (less than a minute), long-lasting (from hours to days) or appear as seemingly distinct events (such as premature beats). In my opinion, the most efficient way to classify arrhythmias would be by mechanism. However, this may not always be possible as the origin of many arrhythmias are still not completely understood or even known. Arrhythmias can either be triggered by a combination of external and internal factors, re-entry or spontaneous events. For instance, arrhythmia can be caused by heterogeneous sympathetic innervation during the formation of scar tissue in diseased hearts (Gardner et al. 2016).

Re-entry occurs when the traveling wave front of the AP collides with a region of tissue that blocks propagation. This region of block can be either physical, like scar tissue, or functional, such as inhomogeneous physical tissue properties. The wave front then propagates around the block and can re-enter the region, and repetitively activate the tissue (Kléber & Rudy, 2004). Under physiological conditions, only one wave of depolarization is obtained per AP firing at the SA node. This is due to the relatively large refractory period of the heart. The refractory period refers to a period during which the muscle cells that have just been excited cannot be re-excited. Absolute refractory period is the time during which the cell is depolarized, the voltage-gated sodium channels are inactivated and cannot initiate a second AP. The relative refractory period begins when the cell membrane potential has just repolarized past the AP threshold: stimulation of an AP at this time is possible but more difficult than normal as the cell is hyperpolarized and voltage gated sodium channels are just beginning to reach the closed state. In the skeletal muscle, the AP duration is of about 2ms and the contraction lasts between 20 to 110ms. This means that in a single contraction, muscle cells can be depolarized many times. These are tetanic contractions and allow for the maximal, sustained muscle contractions. In the heart, tetanic contractions would inhibit blood pumping. This is prevented in cardiomyocytes by the long plateau phase: the AP duration, the absolute refractory period, is of about 250ms which is approximately as long as the cardiac contraction (Bers, 2002). In healthy hearts, immediately after an AP, the cardiac tissue is refractory long enough to force AP propagation in one direction and prevent it from retracing its steps.

In the case of re-entry, normal propagation is either physically or functionally impaired. While a single re-entrant circuit causes tachycardia, several co-existing re-entrant circuits lead to a state called fibrillation, which is characterized by an uncoordinated and repetitive contraction of the cardiac muscle. Atrial fibrillation is the most common serious type of arrhythmia. It is usually asymptomatic but is associated to an increased risk of heart failure and stroke (Munger et al., 2014). Ventricular fibrillation on the other hand, is a much more severe condition as the arrhythmic contractions of the ventricles prevent blood from being expelled. This can quickly be detrimental to other tissues, including the brain and the heart itself, which will not receive constant blood flow and supply of nutrients. Thus, ventricular fibrillation can result in syncope, cardiac arrest and death if prolonged (Baldzizhar et al., 2016).

### 1.2.3: Premature beats

Another possible mechanism for the formation of arrhythmias is the emergence of spontaneous contractions. The SA node is the biological pacemaker of the heart and initiates contractions. However, for many reasons, a contraction can be initiated in a seemingly random area, outside of the SA node. Premature beats are a common arrhythmia, often described by physicians as benign. It is generally asymptomatic but can sometimes be felt as a ‘skipped beat’. They happen naturally, but can be provoked by stress, strenuous exercise or caffeine (NHLIB, 2011). Premature beats are only benign if they happen at low frequency. If frequent, in the atria premature complexes cause an increased risk of atrial fibrillation and heart failure (Lin et al. 2015) and in the ventricles, they can lead to left ventricle dilation (Baman et al. 2010).

Premature complexes may have various origins if they aren’t spontaneous. Certain drugs, such as digitoxin (which is used to treat atrial fibrillation) and catecholamines (which increase cardiac activity), can lead to functional heterogeneity in the myocardium resulting in PVCs. Structural heterogeneity can also be a cause of PVCs: following a myocardial infarction, the scar tissue creates a region of depressed conductivity leading to re-entry and potential premature contractions (Manas & Sumit Verma 2019). Next, early after-depolarizations (EADs) are abnormal depolarizations occurring in the plateau phase or repolarization phase of the cardiac AP. They locally increase action potential duration, causing heterogeneity in the tissue’s properties. The functional heterogeneity caused by EAD in the ventricles can trigger a premature ventricular complex (PVC) (de Lange et al. 2012) and/or re-entry (Scarle & Clayton 2009). If a region of the myocardium is often prone to EADs, it may act as an ectopic focus, triggering premature APs. No matter the underlying cause however, a regularly beating ectopic focus competes with the SA node for activation of the heart. This is called parasystole and it has distinctive electrocardiographic features.

If the PVCs are not sporadic, as in the case of parasystole, their activation pattern are usually described in one of two ways. The notation  $(\textit{number of beats}):\textit{(number of PVCs)}$  compares the number of PVCs to normal beats. For instance, a 5:2 pattern means that in 5 consecutive beats, 2 are PVCs. Next, some patterns are named because of the number of intervening sinus beats

between PVCs (NIBs). The term bigeminy is used when every other beat is a PVC (2:1) and concealed bigeminy is used when all the NIBs are odd (1, 3, 5, 7, 9...). In trigeminy, every third beat is a PVC (3:1) and in concealed trigeminy the NIBs follow a  $3n$  pattern (3, 6, 9, 12, ...),  $3n-1$  pattern (2, 5, 8, 11, ...) or  $3n-2$  pattern (1, 4, 7, 10...) (Moe et Jalife 1977). Similarly, quadrigeminy, pentageminy and hexageminy correspond to a PVC after every fourth, fifth and sixth normal beat respectively.

### 1.3: Parasystole

#### 1.3.1: History

Parasystole was first defined by Fleming in 1912 (Fleming, 1912). Recall, at this time, the electrocardiograph was still under construction and was not readily used by electrophysiologists. Instead, Fleming studied cardiac rhythms using polygraph recordings of radial and carotid arteries (Fig. 2). In this innovative paper, Fleming discusses two cases of possible parasystole. Case 1 is an adult man admitted at the hospital for typhoid fever. The patient showed alternating bouts of heart rate irregularities and normal sinus rhythm. Recordings from this patient's polygraph shows recurring extra-systolic beats, long sequences of uninterrupted sinus beating and beats of intermediate morphology. Case 2 was a 2-year-old boy admitted at the hospital for measles. In this patient, polygraph recordings have shown the same type of irregularity for prolonged times: two normal beats followed by a systolic beat (Fig. 2). In addition, the extra-systolic beats in this patient appeared at a regular cycle length of 1.8s. Fleming suggested that if the ectopic stimulus falls within the refractory period of the heart, it will be ineffective. Consequently, there can be many intervening SA node beats between extra-systolic beats if the timing is right. Fleming also remarks that the periods of the extrasystoles have a common divisor which would be the period of the ectopic pacemaker. In addition to this, he adds another condition to the mechanism of parasystole: the ectopic pacemaker must be in a region 'protected' from the sinus beat. Otherwise, the faster pacing sinus beat would entrain the slower ectopic pacemaker and extrasystoles would never occur.

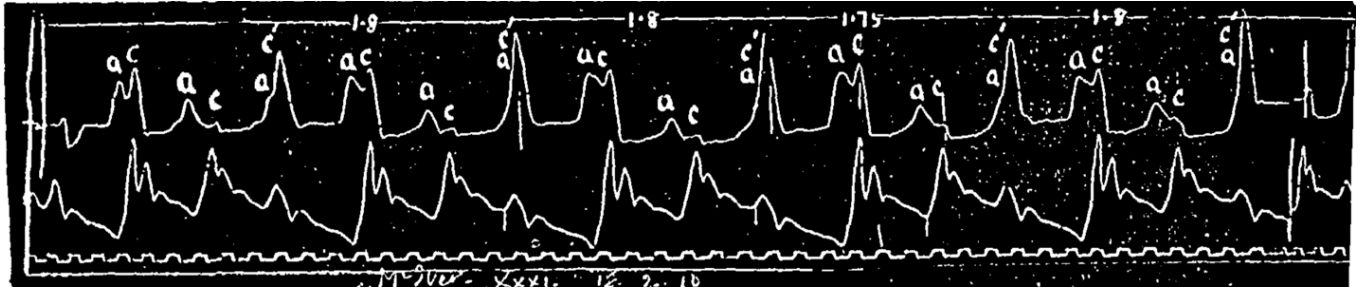


**Figure 2:** Polygraph tracings of radial artery (top) and carotid artery (bottom). Sinus beats are marked by (a), extra-systolic beats are marked by (c). (from Fleming 1912)

Further studies on parasystole have helped determine a set of ‘rules’ for identifying parasystole (Scherf & Chick, 1951):

- 1) There is varying coupling interval (interval between the PVC and the last sinus beat)
- 2) Presence of fusion beats, which occur when the SA node and the ectopic focus fire (almost) simultaneously.
- 3) All inter-ectopic periods have a common divisor that is the period of the ectopic pacemaker.

In addition to this, the ectopic focus was confirmed to be protected from depolarization by the sinus beat. This is due to a region of tissue that tend to propagate waves in only one direction (termed ‘unidirectional block’) surrounding the ectopic focus. In this region of unidirectional block, the AP from the sinus beat cannot enter and activate the region surrounding the ectopic region, but APs from within the ectopic region can escape and depolarize the tissue.

I have defined parasystole as an arrhythmia arising from the interaction of two pacemakers in the heart, competing for activation of the ventricles. I have also mentioned that the ectopic pacemaker should be in a region of depressed conductivity, preventing entrainment by the SA node. However, the AP may not reach the ectopic PM, but electronic variations in the surrounding tissue can affect the pacemaker cycle. Similarly, electronic changes near the SA node from the PVC can impact sinus rhythm. This phenomenon, where the two pacemakers can electronically influence each other is called *modulated* parasystole. Another possibility is that the two pacemakers do not electronically influence each other, either because of distance, functional parameters or a combination of both. In this case, the pacemakers are protected from each other and beat independently, this is referred to as *pure* parasystole. The first parasystole-related papers

were based on ECG recordings of patients with suspected parasystole. These papers provided great insights into the mechanisms of parasystole, however one could not do experimental manipulations and could only analyze clinical data from patients. As the decades passed however, advances in experimental technologies have facilitated the creation of simple, controllable, models of parasystole.

### **1.3.2: Experimental Models**

In 1951, Scherf et al. (Scherf & Chick, 1951) built an experimental model of parasystole in dog hearts. The dogs were anesthetized, and the heart was isolated by removing the sternum, opening the pericardium and severing the vagus nerve. To create a pacemaker focus in the ventricles, a solution of diluted veratrine was applied to the desired region. Veratrine is a mixture of nitrogen-rich alkaloids that reduce conduction velocity in cardiomyocytes. Thus, application of this mixture to the ventricles or atria would result in an increased refractory period in the tissue near the region of application (Swain & McCarthy, 1957). In their study, topical application of veratrine at the surface of the ventricles caused PVCs originating in the area it was applied to. The PVCs lasted for three to five minutes and the researchers observed that three rules of parasystole were respected during this time. The group also noted that when the frequency of the SA rhythm increased, so did the ectopic rhythm. In addition, there were times at which many successive ectopic beats were seen, and the ectopic pacemaker fired at a greater frequency than the sinus pacemaker. In this model, the ectopic focus is likely created as a result of re-entry: the low conduction due to veratrine creates a functional block at the site of application on the ventricles. As the AP travels around the site of block, it can curl back in and elicit a PVC from this region. This mechanism explains why the ectopic rate increases as the sinus rate increases. It would also explain why there were periods during which the ectopic beat was faster – the re-entrant wave keeps curling in. Even though this model showed the three main characteristics of parasystole, the high frequency of the ectopic focus is an important difference from clinical studies, where the parasystolic foci are slower and successive PVCs are rare.

The Jalife group in New York, 25 years later, developed another experimental model using Purkinje fibers (Jalife & Moe, 1976). The group isolated free-running false tendons, made of

cardiac muscle, Purkinje fibers and blood vessels (Kervancioğlu et al., 2003), from canine ventricles. The fiber was separated into three chambers. Chamber 1 is a short segment of about 1mm in a low potassium (2mM) environment. The low potassium increases the pacemaker potential and so chamber 1 fires at a fast rate and so, this chamber will be the main pacemaker. Chamber 2 segment is 2mm long and is perfused with a sucrose solution. This serves as a region of reduced conduction velocity and is used to model entrance-block. Chamber 3, 1mm long, is perfused in 4mM (physiological) potassium, and so fires at lower intrinsic rate than chamber 1 and will thus represent the ectopic pacemaker. Their paper included three experimental groups. In the first, chambers 1 and 3 were left to beat spontaneously and electrodes were used to record the activity. This resulted in a 4:1 block: an AP in chamber 3 is triggered for every 4 APs from chamber 1. APs from chamber 1 caused small depolarization in chamber 3 that occurred earlier in the ectopic pacemaker's cycle with every AP until it was early enough to elicit an AP. When chamber 3 discharged, electronic influences traveled to chamber 1, as a small depolarization. The group noted that if this depolarization arrives early in the cycle of chamber 1, the next AP was delayed. On the other hand, if the depolarization arrived late in the cycle, it elicited an earlier response. They studied this phenomenon in the second experimental group: chamber 3 was electrically stimulated at different times in the main pacemaker's cycle. For each stimulus from the ectopic pacemaker, they recorded the change in cycle length of the main pacemaker. As expected from the first experimental group, stimuli occurring in the first half of the cycle delayed the next expected beat and stimuli occurring in the second half of the cycle accelerated, or captured, the next beat (Fig. 3). This biphasic curve is commonly referred to as the phase-resetting curve (PRC). In the third set of experiments, current pulses of defined amplitude and duration were injected in chamber 3. These pulses, just like the stimuli above mentioned delayed or accelerated the next main pacemaker beat depending on their timing in the cycle. With this simple model using Purkinje fibers, Jalife et al. concluded that in modulated parasystole, despite the decreased conduction velocity protecting the ectopic pacemaker, electronic modulations from the ectopic pacemaker can reach and modulate the main pacemaker in a predictable fashion, as shown by the PRCs.

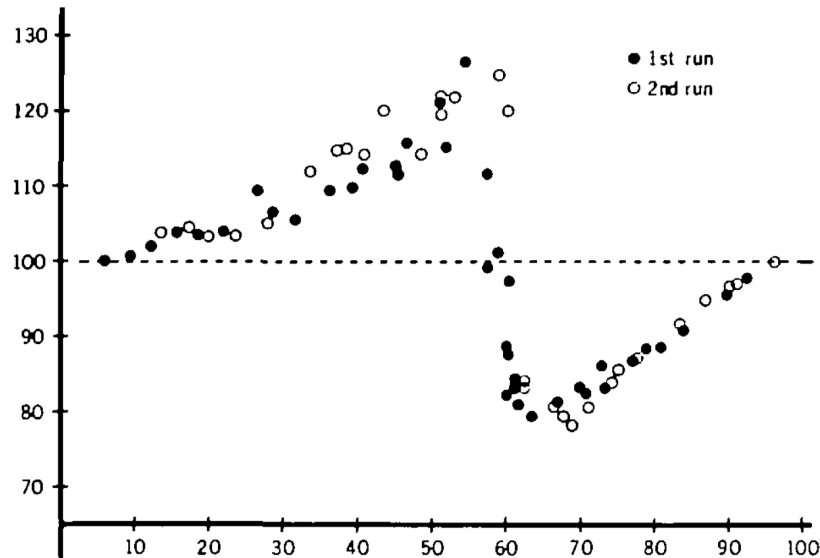


**Figure 3:** Delay and acceleration of main pacemaker as a function of coupling interval. Ectopic Stimuli was applied every 10 to 15 spontaneous beats (from Jalife et al. 1976)

Jalife et al. in 1980 ran another set of experiments based on the Purkinje fiber model described above. This time, they analyzed a specific phenomenon called reflection (Antzelevitch et al., 1980). Reflection is a type of re-entry that occurs when an AP from the main pacemaker travels to depolarize the ectopic focus and immediately travels back to the main pacemaker to depolarize it once again. This can only happen in certain conduction conditions where the sum of the delay from the main pacemaker to the ectopic pacemaker and from the ectopic pacemaker back to the main pacemaker is greater than the refractory period of the main pacemaker. Otherwise, the reflection falls in the refractory period of the main pacemaker and is only expressed as a small depolarization if it is expressed at all. To fine tune the level of conductivity in the sucrose gap, a shunt was placed. The resistance in this shunt could be controlled and so increases in shunt resistance reduces conductivity and decreases in shunt resistance increases conductivity. Their results show that reflection can be obtained over a limited range of shunt conductivity. At a shunt resistance of  $12\text{k}\Omega$  there is no reflection: at very low conductivity only small electronic influences can travel. In contrast, at a shunt resistance of  $5\text{k}\Omega$ , conductivity was high enough for reflection to occur. Once the parameters for reflection had been established, the authors note that the observed firing dynamics depend on the cycle length of the main pacemaker: increasing the main pacemaker's cycle length resulted in a change in the observed dynamics, from bigeminy to

trigeminy for instance. They conclude that re-entry and reflection are dependent on conduction characteristic and even though they have similar behavior as parasystole and can serve as a simple model of parasystole, in the human heart they are distinct phenomena. In parasystole, unidirectional block is necessary but bidirectional conduction is required for reflection re-entry to occur. Next, there needs to be a spontaneous activity in parasystole and this is not always the case for reflection.

These experiments support the theory of modulated parasystole and the PRC is a proof that small electronic interactions can modify pacing activity.

### **1.3.3: Mathematical models**

Despite providing a great insight into the problem of parasystole, experimental models have some considerable constraints. A limited number of experiments can be carried out since studies in an intact heart are challenging. In addition, it was preferable to work with a more accessible compartment of the heart (such as Purkinje fibers). Experimental models also have a limited lifespan and greatly depend on the isolated tissue's viability. In the 1970's computer technologies had advanced to the point where they became readily available to scientists. Computer technologies allow for the implementation of mathematical models and the simulation of very large data sets that can be analyzed and so, researchers were no longer limited to results from experimental or clinical studies. With mathematical models, researchers have complete control over their model's parameters and their experiments aren't subject to the unpredictable fluctuations of biological tissue. In parallel with the experimental studies, there have been a number of theoretical models developed for pure and modulated parasystole.

Moe and Jalife, developed a mathematical model of modulated parasystole a year after their experimental results were first published (Moe & Jalife, 1977). The model consisted of two pacemakers, one representing the SA node (SN) and another representing the ectopic pacemaker (EP). The simulations were run by updating equations, where the time between updates, called the time-step, is scaled to match physiological parameters. In this model, the size of 1 time-step was set to 20msec. The period of SN was fixed at 40 time-steps, the refractory period was 15 time-

steps and the period of EP was varied between 60 and 150 time-steps. If EP fires outside the refractory period of SN, the next SN beat was silenced: this is called a compensatory pause. The group also programmed many PRCs of varying maximal amplitudes. Their results (Fig. 4) show that not only do the observed dynamics depend of the ectopic cycle length, as previously demonstrated in experimental models, but the shape of the PRC, which reflects the intensity of electronic modulation, also affects the observed dynamics. Large electronic modulations between pacemakers give rise to simple dynamics but as the electronic modulations decrease, more complex rhythms are observed.

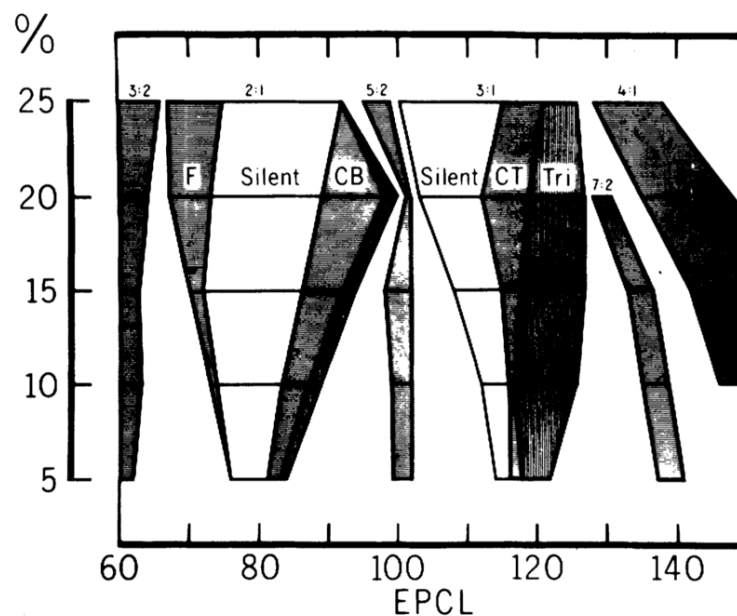


**Figure 4:** *Entrainment zones as function of ectopic pacemaker cycle length (EPCL) and maximal amplitude of programmed PRC (as % of EPCL). F = fusion beats, Silent = No PVC, CB = Concealed bigeminy, CT = Concealed trigeminy, Tri = Trigeminy. Blank areas are regions with complex dynamics (from Moe et al. 1977)*

In 1986, Jalife et al. applied their mathematical model to clinical records (Jalife et al., 1986). They built a PRC from clinical records of a patient with apparent extrasystolic beats originating in the atria, near the SA node. Applying this PRC to their mathematical model, the frequency-dependent dependent arrhythmic behaviors obtained greatly matched that of the real clinical records. We thus have here a model of modulated atrial parasystole, confirming the possibility of phase resetting in parasystole.

An alternative model was proposed by the Ikeda group in 1981 (Ikeda et al., 1981). Unlike in Jalife et al. 1977, where every ectopic beat is followed by a compensatory pause, this model is more complex and includes many assumptions and equations to also allow for interpolated ectopic beats (an ectopic beat followed by the scheduled sinus beat, i.e.: no compensatory pause), and fusion beats. Thus, compensatory pauses only occur if the time between the scheduled sinus beat and the ectopic beat is smaller than the refractory period. From a defined PRC and ratio of cycle lengths, this model can predict the observable excitation patterns. In 1983, the same group published further results of their mathematical model as applied to ventricular parasystole (Ikeda et al. 1983). In the paper, the authors analyzed the predicted patterns for a large set of parameters. Their model yielded dynamics seen in clinical recordings such as silent beats, concealed bigeminy or trigeminy, bigeminy, trigeminy or quadrigeminy, interpolated beats and complex rhythms that do not fit in any of the aforementioned groups. In addition, as seen in the experimental models, as the ratio of ectopic cycle length to SA node cycle length increases, we see a migration of dynamics from bigeminy, to trigeminy to quadrigeminy. Thus, this detailed model gives a mathematical basis for the observed dynamics and further supports the proposed mechanism of parasystole.

Next, in 1989, Hoshino et al. published a hybrid model of parasystole based on an earlier experimental model by Antzelevitch et al. In the experimental model, an intact *in situ* canine heart was connected to a Purkinje fiber sucrose-gap preparation, acting as the ectopic pacemaker (Antzelevitch et al. 1983). Similarly, Hoshino et al. connected to the intact heart a microcomputer that acts as the ectopic pacemaker (Hoshino et al. 1989a). Replacing the Purkinje fibers by a computer allows for greater parameter freedom and control as entrance-block and the degree of modulation (the PRC) can be varied on a greater range than in the experimental model alone. Moreover, in order to reduce fluctuations in the sinus rhythm, the SA node in the canine heart was crushed and the right atrium was electrically paced. Interestingly, instead of varying the ectopic cycle length, here the sinus cycle length was varied while the ectopic rhythm stayed constant (unless there is modulation). Nevertheless, the observable dynamics are as expected from previous papers: as the ectopic to sinus cycle lengths ratio increases, we see an evolution from bigeminy, to trigeminy, to quadrigeminy and even pentageminy. This shows that even if the ectopic cycle length is constant, the excitability patterns are heart rate dependent in modulated parasystole. In another

paper, this same group (with the same hybrid model) have tested a specific, asymmetrical PRC that has a short delay phase and a long accelerating phase (Hoshino et al. 1989b). With this particular set of parameters, the group showed that re-entry can occur as the ectopic focus is often captured by the sinus beat (because of the particular PRC) and this can result in ventricular tachycardia. Hence, with this innovative hybrid model, the group has shown the relative importance of the heart rate and PRC in determining the excitation patterns and the possibility of detrimental arrhythmias rising from the presence of an ectopic focus.

In 2004, Loskutov et al. published another complex and detailed model based on a system of nonlinear difference equation (Loskutov et al. 2004). In this case however, the two pacemakers are mutually interacting, and each can be modulated by the other. This high-resolution model confirms observations previously made regarding modulated parasystole: the ratio of the cycle length of the ectopic pacemaker to the cycle length of the main pacemaker and the level of modulation between the pacemakers are the main factors that govern the wave dynamics. This is yet another paper that confirms and supports the theory of modulated parasystole and it also suggests that in order to fully understand the problem, mathematics and physics methods need to be used.

Mathematical models for pure parasystole assume no electronic modulation between the pacemakers. This situation may seem overly simplified as even when separated by a region of block, small electronic fluctuations can travel in the tissue and affect the electronic milieu of either pacemaker, which will modify pacemaker activity (Jalife et al. 1980). However, Glass et al. in 1986 have shown that even the simplest circumstances of parasystole yield interesting yet predictable dynamics (Glass et al., 1986). In their model, they assume two independently beating pacemakers. One is the sinus pacemaker of period  $S$ , the other is the ectopic pacemaker of period  $E$ . The refractory period after a sinus beat is  $\theta$ . In the model, a compensatory pause is imposed after every ectopic discharge. The analysis was conducted by varying the ratios  $E/S$  and  $\theta/S$  and recording the number of intervening sinus beats between extra-systolic beats (NIBs). From simulations and analytic results, the authors have proposed a set of rules for the NIBs observed in pure parasystole:

- 1) There are at most three different values of NIBs for any set of parameters.

- 2) One and only one of these is odd.
- 3) The sum of the two smallest values is equal to one less the other value.
- 4) Considering the sequence of all NIBs over time, only one of the three values can repeat itself.

These rules were apparent in all of their simulations and have thus been proposed to be characteristic of pure parasystole. However, the authors have noted that rule 4 isn't maintained in some previous recordings of parasystole and this rule can be omitted when trying to identify parasystolic patterns. Next, their simulations and analytical results also allowed the group to predict expected NIBs depending on the E/S and the  $\theta$ /S ratios (Fig. 5). This figure was built using Farey's sequence. A Farey sequence of order  $n$  is a sequence of reduced fractions between 0 and 1 where the highest denominator is  $n$ . For example, Farey's sequences of orders 2 and 4 are  $\{0/1, 1/2, 1/1\}$  and  $\{0/1, 1/4, 1/3, 1/2, 2/3, 3/4, 1/1\}$  respectively. The Farey diagram is constructed by drawing a square where the bottom line is an axis of the Farey sequence, from 0 to 1. Next the diagonals are drawn, from  $0/1$  to the top right corner and  $1/1$  to the top left corner. At the Farey number  $1/2$ , two lines towards the two closest corners are drawn. The following lines are drawn according to increasing denominator ( $1/2; 1/3; 2/3; 1/4; 3/4 \dots$ ) with two lines per Farey number, each going to the nearest corner. The segments from the Farey numbers yield triangular regions of NIBs, as we increase the order of the Farey sequence smaller regions of higher value NIBs regions can be seen. In Fig.5, the authors have combined units of Farey diagrams of order 3 in order to provide a spectrum of NIB evolution along E/S ratios, from 1 to 4. Despite simplifying the problem of modulated parasystole, this model yields important conclusions that are worth exploring as they could give insight on the more complex modulated parasystole model. Eleven years later, Saoudi et al. explored the model of pure parasystole in humans as just explained (Saoudi et al., 1995). Here, the group electrically stimulated the atria and ventricles of six cardiovascular patients suspected to have supraventricular arrhythmias. In all patients, the atria were electrically paced at a constant rate while the ventricles were paced at different rates (for different runs) and the NIBs were recorded. A total of 50 suitable runs were obtained: 48 showed NIBs that followed the rules and matched the predictions as described by Glass et al. In the two cases that diverged, the E/S ratio was 1.33 and only two values of NIBs were seen: 2 and 0. This would suggest that the simple model of pure parasystole is applicable to the human heart and

dynamics of the modulated parasystole could simply be deviations from the pure parasystole model.

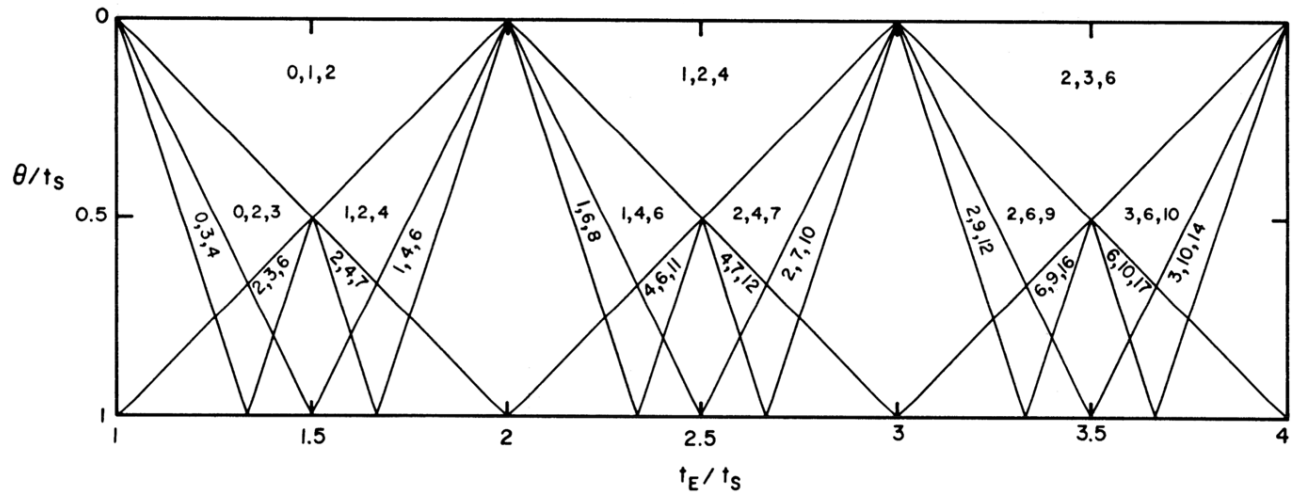


**Figure 5:** Allowed values of NIB depending on  $E/S$  and  $\theta/S$  values. Farey diagrams of order 3. (from Glass et al. 1986)

All of these models suggest that parasystole can present itself in a variety of different patterns in an ECG. It is thus relevant to fully understand the mechanisms of both pure and modulated parasystole as PVCs are often associated with an increased risk of cardiac disease or sudden cardiac death (Baman et al., 2010).

#### 1.4: Rationale and goal

The theoretical models above described, despite providing us with a greater understanding of parasystole, lack a very important aspect: space. In the real heart, the sinus and the ectopic pacemakers are in separate locations but are connected by excitable non-pacemaking tissue. This tissue carries electrical impulses from one pacemaker to the other and creates a small delay in the transmission. It is thus conceivable that the addition of an excitable tissue in the theoretical models can bring a greater degree of variability in the observable patterns, which in turn will deepen our knowledge of parasystolic dynamics. In this thesis, I consider theoretical models of parasystole that include spatial separation of pacemaking sites.

I have studied two models. The first model is a discrete model in space and time: a cellular automaton (CA). This model allows for a direct mapping of key physiological parameters to user defined variables and is computationally efficient. The second model is continuous in time and based on the Fitzhugh-Nagumo (FHN) differential equations. The FHN model was first introduced in the 1960s. It is an adaptation of the Van der Pol oscillator with two variables: one representing excitability and the other refractoriness (Fitzhugh, 1961).

## CHAPTER 2: CELLULAR AUTOMATON MODEL

### 2.1: Methods

The cellular automaton (CA) is a grid of discrete live cells that have states changing through time depending on a set of predetermined rules. This parasystole CA model is adapted from Bub et al. 1998. Here, we model a line of  $N$  cells where states  $1, 2, \dots, E$  are excitatory, states  $E+1, E+2, \dots, E+R$  are refractory and state  $0$  (also corresponding to state  $E+R+1$ ) is inactive. The states are updated at every time step such that:

$$\begin{aligned}
 & \text{if } 1 \leq \text{state}^t \leq E + R: \\
 & \quad \text{state}^{t+1} = \text{state}^t + 1 \\
 & \text{if } \text{state}^t = 0: \\
 & \quad \text{if } n > 0: \text{state}^{t+1} = 1 \\
 & \quad \text{else: } \text{state}^{t+1} = 0
 \end{aligned}$$

where  $n$  corresponds to the number of neighboring active cells. As a 1D line of cells is simulated here, the neighborhood of a cell corresponds to the immediate cell to the left and the one to the right. If one or both of these cells are active ( $n > 0$ ), the cell becomes active at the next update.

The CA model is run using the programming software Python 3.7.6. The libraries used are: *numpy*, which allows for creation and manipulation of multi-dimensional arrays, *pandas* which allows for large data manipulation and for creating and reading Excel files and *plotly* that allows for production of interactive, high-quality graphs. All the other functions employed in the simulation are my own. The pacemakers are set to ‘fire’ at fixed time-step intervals: the faster pacemaker represents the sinus node (SN) and the slower pacemaker is the ectopic pacemaker (EP).

Using data from middle eastern men and women the adult human heart, from the top of the atria to the apex of the ventricles, measures about 12cm (Mohammadi et al. 2016) and the conduction velocity in the myocardium is of about 50cm/s (Yuniarti et al. 2017), thus, the electrical impulse travels from the SN to the apex of the heart in about 0.24s (or 240ms). Consequently, in this model, we will have a line of 241 cells, SN at cell #1 and EP at cell #241 such that it takes 240

time-steps for the SN impulse to reach the EP. Hence,  $1dt = 1ms$  and  $1dx = 0.5mm$  in our model and EP is assumed to be at maximal distance from SN.

The input parameters in the model are the number of cells ( $N$ ), number of time-steps to run ( $\#dt$ ), position of SN ( $SN_x$ ), position of EP ( $EP_x$ ), SN cycle length ( $T_{SN}$ ), ratio of EP cycle length to SN cycle length ( $R = T_{EP}/T_{SN}$ ) and ratio of the refractory period to SN cycle length ( $\theta/T_{SN}$ ). To match the above-mentioned physiological parameters, we set for all simulations:  $N = 241$ ,  $SN_x = 1$  and  $EP_x = 241$ , where  $T_{SN}$ ,  $T_{EP}/T_{SN}$  and  $\theta/T_{SN}$  are varied throughout the simulations.

## 2.2: Results

### 2.2.1: Characteristics of model

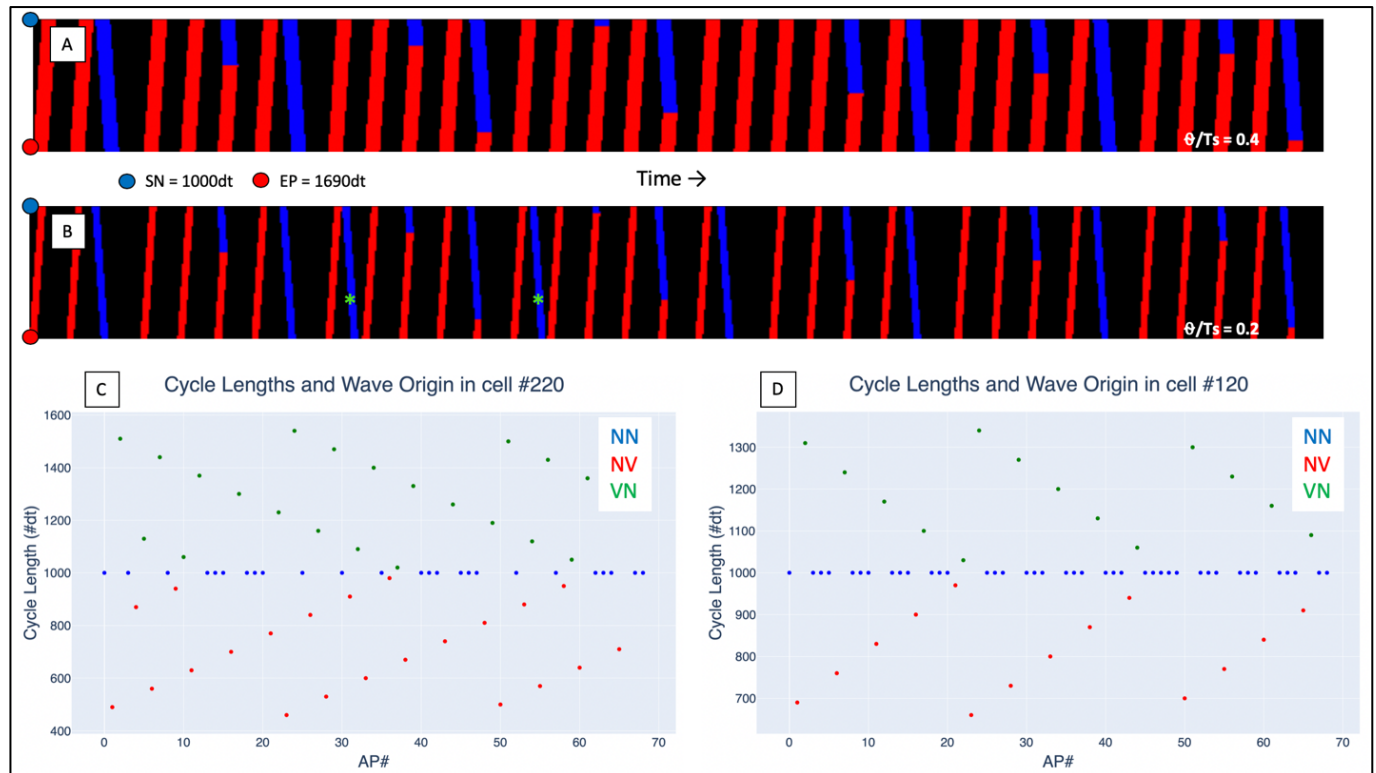


**Fig. 6:** Cellular Automaton model. A) Space-time plot with  $T_{SN} = 1000dt$ ,  $T_{EP} = 1690dt$  and  $\theta=400dt$ . B) Space-time plot with  $T_{SN} = 1000dt$ ,  $T_{EP} = 1690dt$  and  $\theta=200dt$ . C) Cycle length plot for cell # 220 from panel A. D) Cycle length plot for cell #120 from panel A

As the model represents a 1D line of cells, we can plot the results in a 1D lattice where each line corresponds to a cell and each column to a time-step. This is represented in the space-time plots in Figs. 6A and 6B: waves originating from the SN are shown in red and waves originating from the EP are in blue. In these figures, we have  $T_{SN} = 1000dt$  and  $R = 1.69$ . This shows that some EP beats can propagate from the ectopic pacemaker, activating the neighboring cells and the distance travelled by each ectopic beat varies. In panel A, we have  $\theta/T_{SN} = 0.4$  and  $\theta/T_{SN} = 0.2$  in panel B. The smaller refractory period in panel B allows for the appearance of interpolated beats (green stars in Fig 6B): EP beats that do not result in a compensatory pause. These EP beats are only visible when the refractory period is short enough to allow the EP beat to travel back to SN before the next scheduled beat.

Next, in Fig. 6C the cycle lengths for the cell #240, the cell immediately next to EP, are plotted. The first thing to note is that the cycle lengths aren't constant, but instead seem to oscillate in a periodic manner, with most cycle lengths corresponding to the  $T_{SN}$ . The dots are also color coded (see the figure legend), where N corresponds to a SN wave and V is an EP wave and so, NN are SN beats preceded by a SN beat, NV are EP beats preceded by a SN beat (i.e. the coupling interval) and VN are SN beats preceded by an EP beat. NV is always smaller than  $T_{SN}$  as it is the result of a premature beat and VN is always greater than  $T_{SN}$  because of the compensatory pause. Consequently, we get  $NV + VN = 2NN$ , the time interval from a sinus beat to the ectopic beat plus the time interval from that ectopic beat to the following sinus beat is twice the sinus cycle length. However, for interpolated beats, we have  $NV + VN = NN$  as there is no compensatory pause. Moreover, since the EP wave travels a different distance every time it manages to escape the refractory period, the cycle length oscillations also vary in space for cells far from the pacemaker, as seen in Fig 6D which plots cell #120. The oscillations in cell #120 are dampened (note y-axis scale) and there are 22 ectopic beats at cell #240 as opposed to 14 at cell #12, for the same time-frame.

## 2.2.2: NIB evolution in space

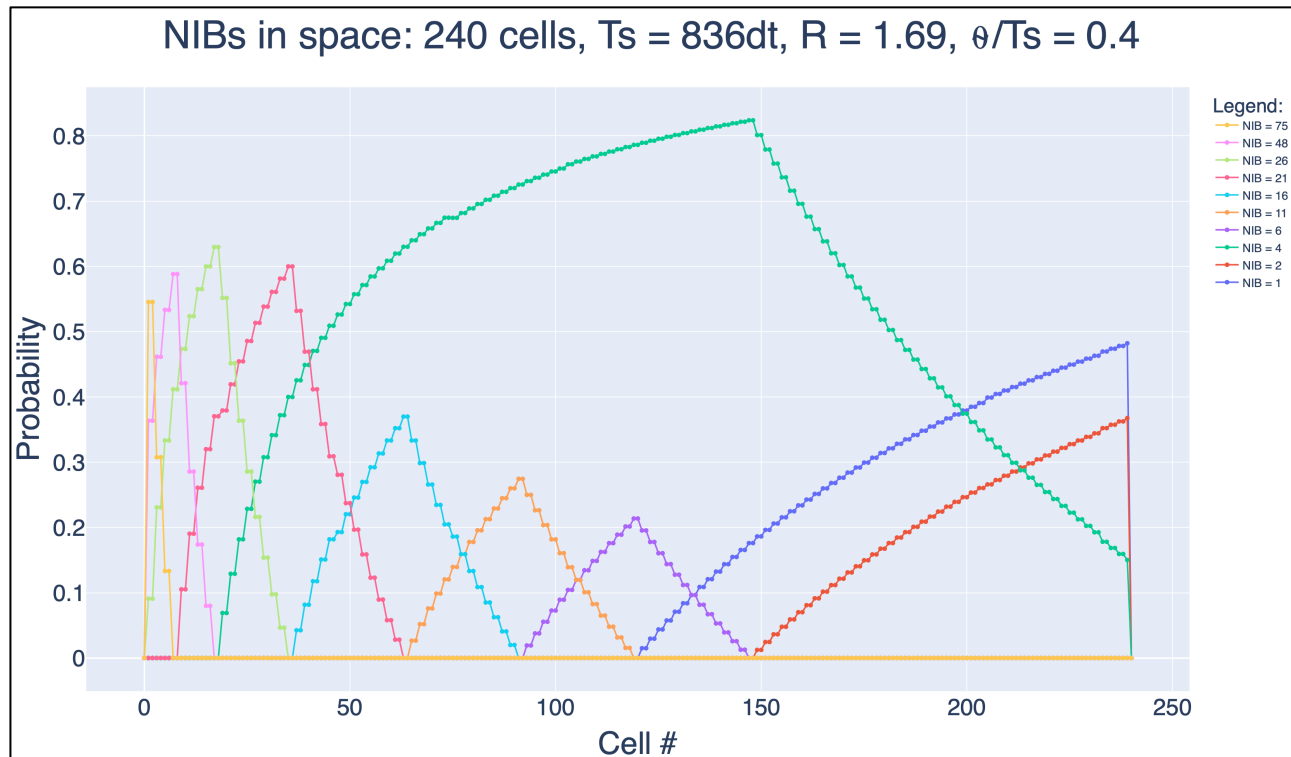


**Fig. 7:** Cellular Automaton model. Number of intervening beats (NIB) evolution in space for  $T_{SN} = 836dt$ ,  $T_{EP} = 1412dt$  and  $\theta = 334dt$

Since the EP beats are blocked at different points in space, NIBs vary in space. In Fig. 7, we have  $R = 1.69$  and  $\theta/T_{SN} = 0.4$  and we can observe the evolution of the probability of NIBs in space. From this figure, we can see that at any point in space, there are at most 3 different NIB values and these values seem to follow the pure parasystole rules earlier described. In Fig. 8, we have a similar plot as above described with parameters  $R = 1.84$  and  $\theta/T_s = 0.2$ . These settings allow for the emergence of interpolated beats and this results in intermediate NIB values as seen in the graph. In all regions of the line of cells, there are 4 NIBs: 3 of those follow the NIB rules and the last value is an intermediate between the two highest NIB values. For instance, at cell #50 have NIB values (1,8,9,10): (1,8,10) is a valid triplet and 9 is between 8 and 10 and similarly, at cell #100 we have (1,6,7,8): (1,6,8) is a valid triplet and 7 is between 6 and 8. Interpolated beats thus cause small deviations from the predictions in pure parasystole in Glass et al. (1986).

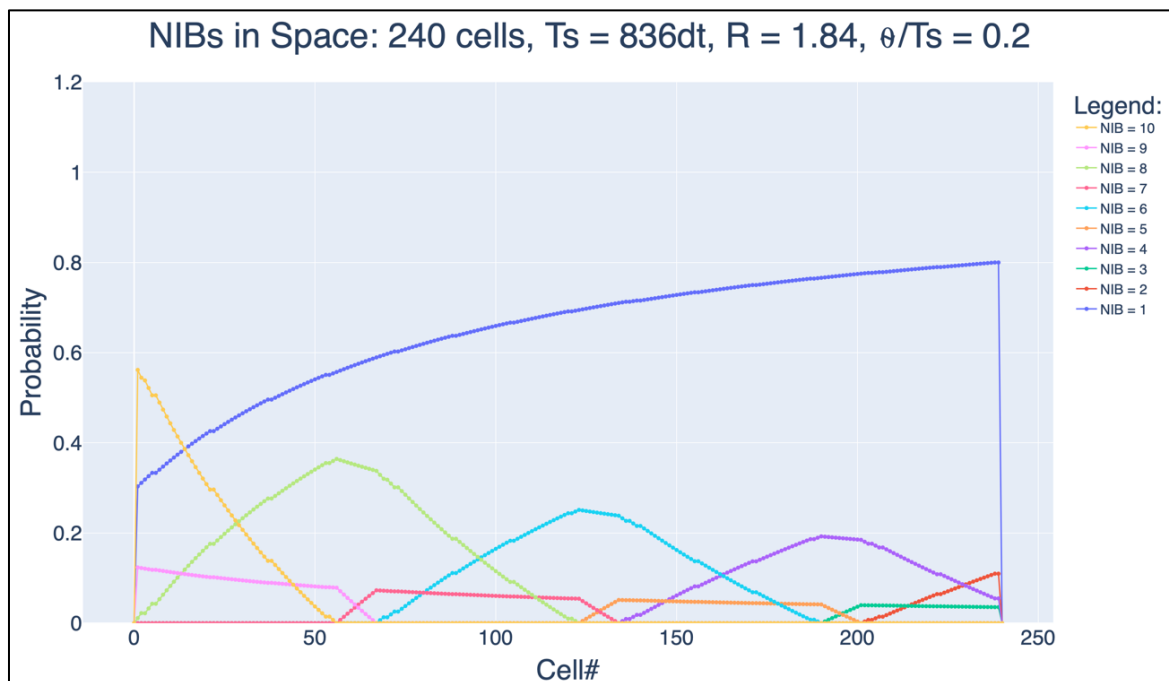


**Fig. 8:** Cellular Automaton model. NIB evolution in space for  $T_{SN} = 836dt$ ,  $T_{EP} = 1538dt$  and  $\theta = 167dt$

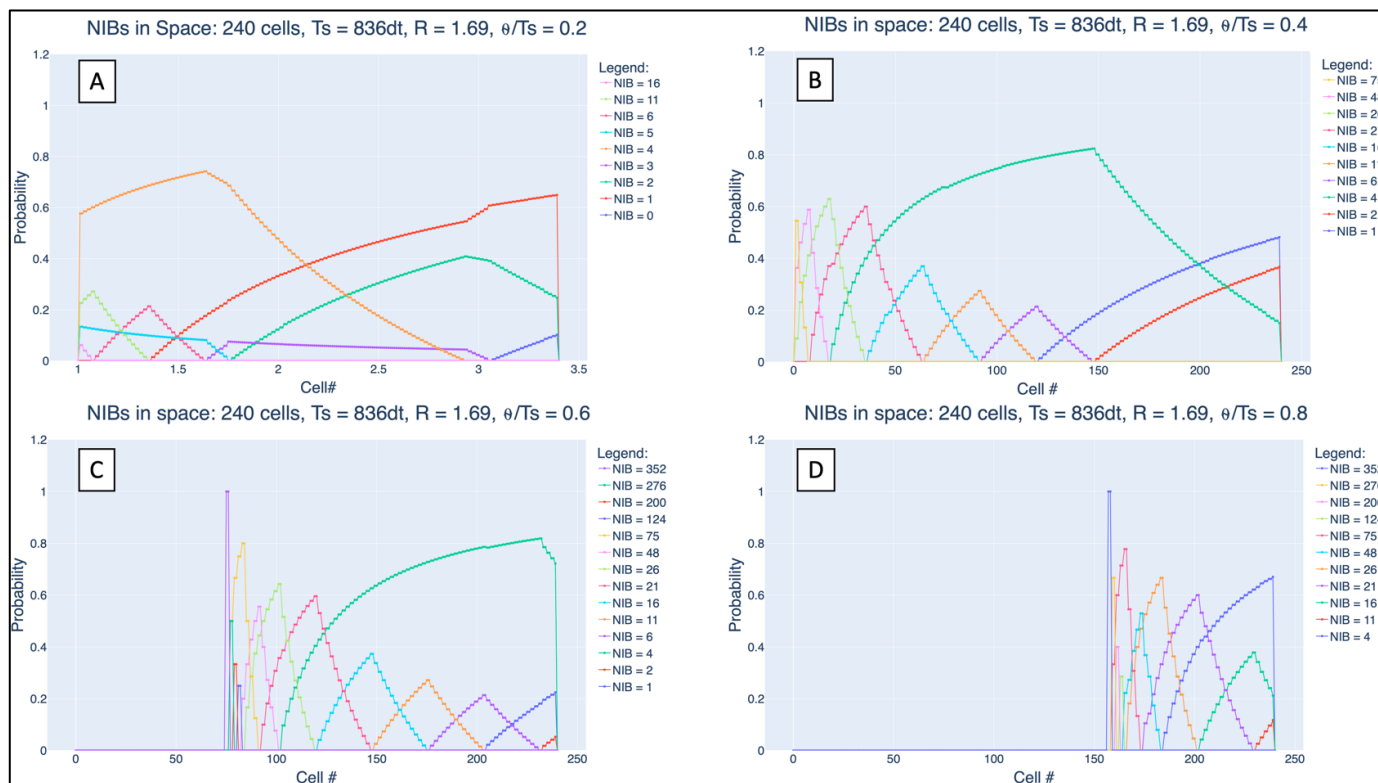


**Fig.9:** Cellular Automaton model. NIB evolution in space for  $T_{SN} = 836dt$ ,  $T_{EP} = 1412dt$ . A)  $\theta = 167dt$ . B)  $\theta = 334dt$ . C)  $\theta = 501dt$ . D)  $\theta = 668dt$

Next, we analyze the correspondence of space to NIBs. In Fig. 9 I have plotted NIB evolution in space for 4 values of  $\theta/T_{SN}$  (0.2, 0.4, 0.6 and 0.8, respectively panels A, B, C and D) and all other parameters remained fixed ( $T_{SN} = 836dt$ ,  $R = 1.69$ ,  $N = 241$  cells and  $\#dt = 600,000$ ). Note that at  $\theta/T_{SN} = 0.2$ , we can see intermediate NIB values due to interpolated beats. At the EP (cell #241), omitting interpolated beats, the NIBs match those predicted by the pure parasystole model (Fig. 5): (0,1,2) at  $\theta/T_{SN} = 0.2$ , (1,2,4) at  $\theta/T_{SN} = 0.4$  and (1,2,4) at  $\theta/T_{SN} = 0.6$ . From the four panels of Fig. 9, the NIB sequence in space for  $R=1.69$  is (0,1,2), (1,2,4), (1,4,6), (4,6,11), (4, 11,16), (4, 26,21), ..., (75, 124, 200), (124, 300, 325) and it is shifted as  $\theta/T_{SN}$  increases such that the NIB triplet at EP corresponds to the pure parasystole predictions. The Farey diagram in Fig. 10 is constructed like the one in Fig. 5 by Glass et al., however, we have added two more levels (Farey diagram of order 9) to show some smaller regions of higher NIB values. The sequence from Fig. 9 corresponds to the NIB sequence as  $\theta/T_{SN}$  is increased for  $R = 1.69$  (green line, Fig. 10) and these results suggest that increasing the recording distance from the pacemaker corresponds to increasing the refractory period at the pacemaker. Thus, some points can be far enough from the pacemaker so that the refractory period is so high, that EP depolarizations cannot reach them. Such regions can be seen in panels C and D of Fig. 11: in the region close to SN (cell#1) where there are no NIB values. The furthest region that can be reached by an EP wave is given by the equation:

$$x = \frac{1}{2}(2N + \theta - T_{SN}) \quad (1)$$

where  $x$  is the number of cells from SN,  $N$  is the number of simulated cells,  $\theta$  is the refractory period (in  $\#dt$ ) and  $T_{SN}$  is the period of SN (in  $\#dt$ ). Note that if  $x < 0$ , this means that the EP wave can depolarize the entire line of cells and if  $x > 0$ , then there is a limit to how far the EP wave can travel within the line of cells. The latter is valid if and only if  $2N + \theta > T_{SN}$ . For a given  $T_{SN}$ , as the refractory period is increases,  $x$  in Eq. (1) increases and the maximum penetration of the ectopic beat decreases.

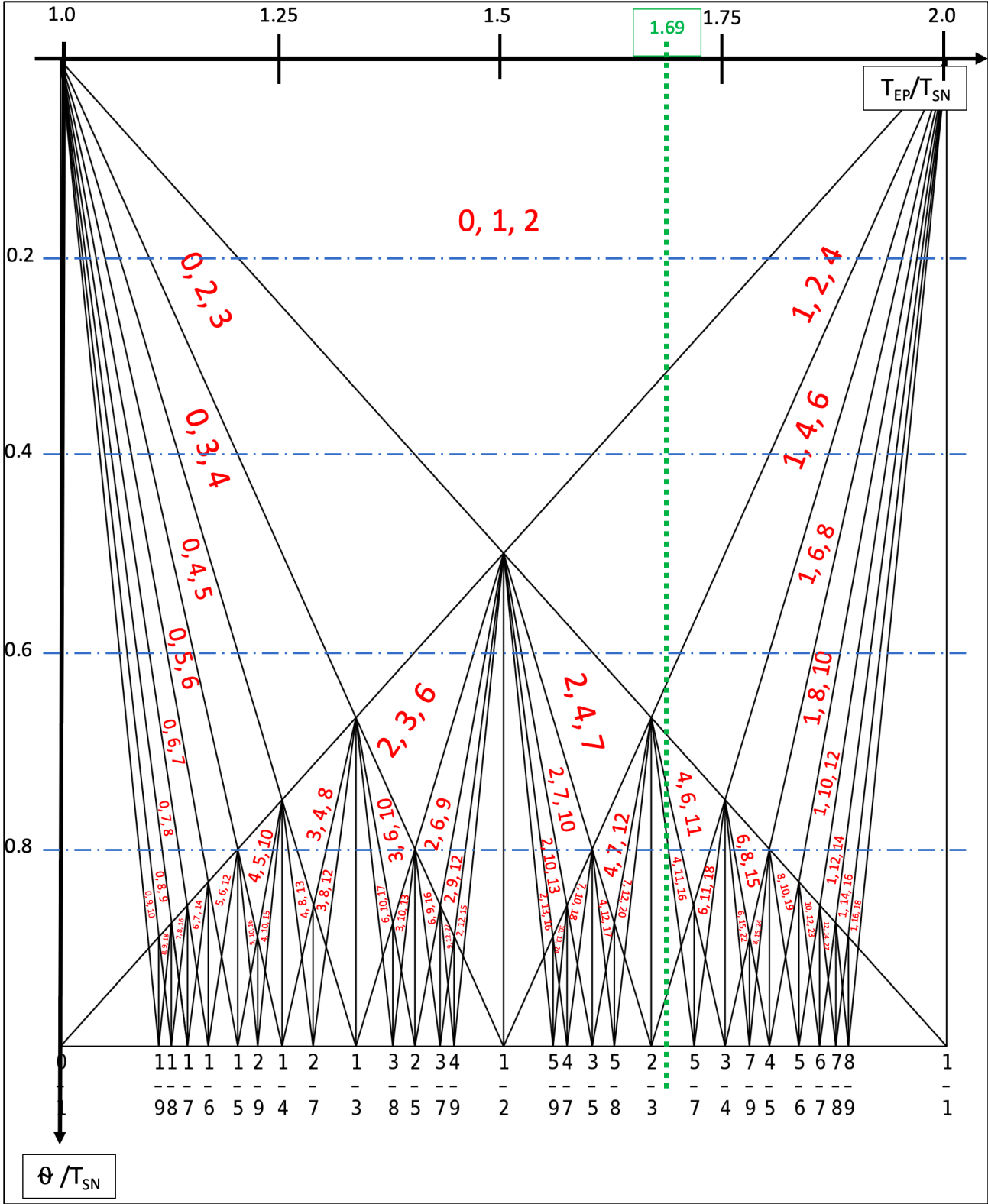
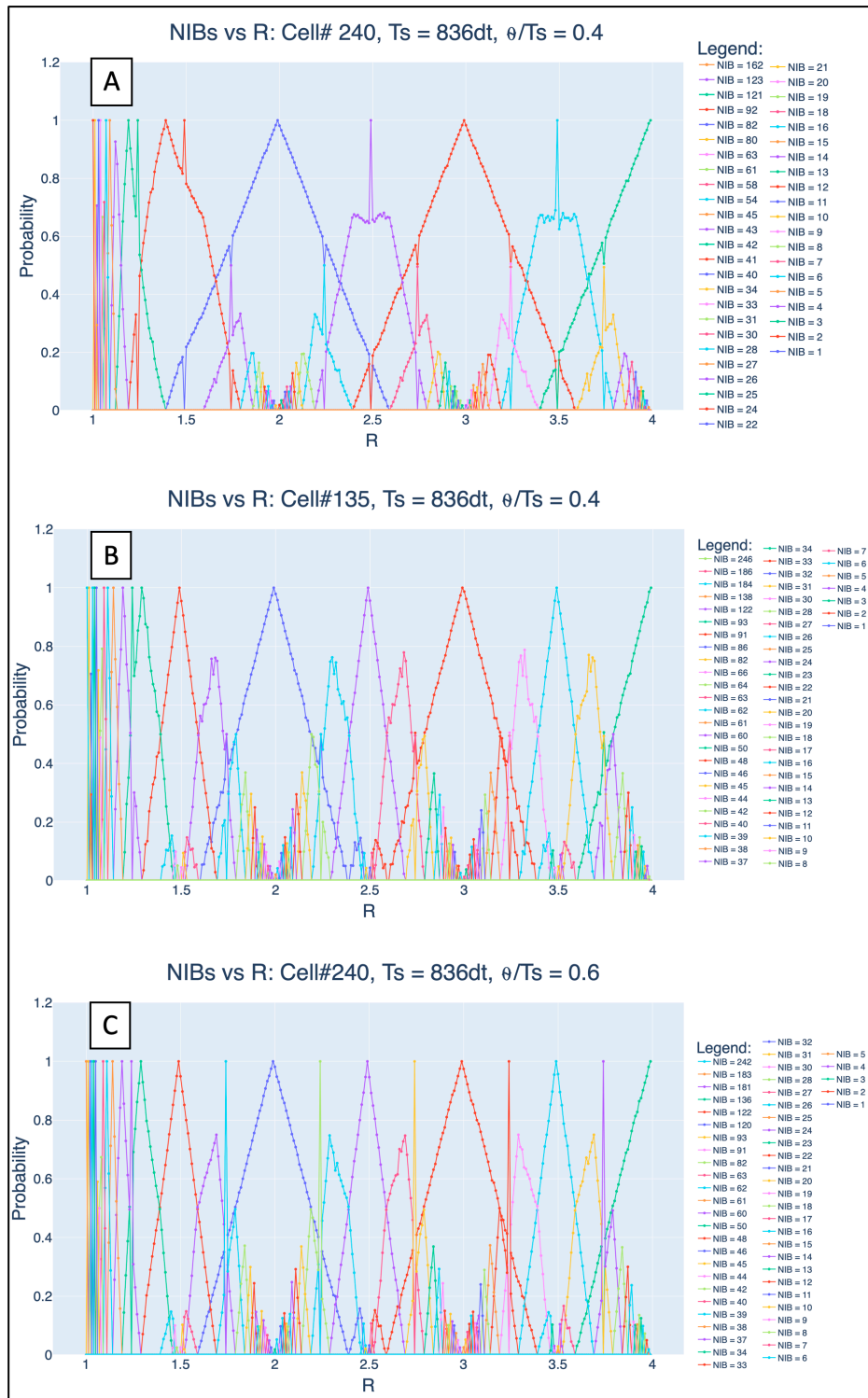


Fig. 10: Farey diagram of order 9 and corresponding NIB regions. Vertical green dashed line:  $T_{EP}/T_{SN} = 1.69$

From Figs. 7, 8 and 9, four parasystole behaviors for non-adjacent pacemakers can be observed:

- 1) At any point in space, there are exactly three possible NIB values and the last occurrence of a NIB is immediately followed in an adjacent cell by the first occurrence of another NIB.
- 2) Without interpolated beats, all NIB triplets observed follow the pure parasystole rules earlier described (except for rule 4).
- 3) The evolution of NIBs in space, as we get further from the EP seems to correspond to the NIB evolution in the pure parasystole model as we increase  $\theta/T_{SN}$  (Glass et al., 1986).
- 4) For two pacemakers SN and EP separated by a line of N cells,  $x = \frac{1}{2}(2N + \theta - T_{SN})$ , where x is the numbers of cells from SN where the EP wave travels the furthest.

2.2.3: NIB vs  $T_{EP}/T_{SN}$



**Fig. 11:** Cellular Automaton model. NIB evolution with  $T_{EP}/T_{SN}$ . A) NIBs at cell #240 for  $T_{SN} = 836dt$   $\theta=334dt$ . B) NIBs at cell #120 for  $T_{SN} = 836dt$   $\theta=334dt$ . A) NIBs at cell #240 for  $T_{SN} = 836dt$   $\theta=501dt$ .

We now compare the NIB evolution with  $R$  in Fig. 11A, B and C. Panels A and B, correspond to cells #240 and #135 respectively for  $R = 1.69$  and  $\theta/T_{SN} = 0.4$ . At cell#240, the distribution of NIBs once again matches the predictions made by Glass et al. in 1986 (Figure 3A of their paper), which further suggests that the dynamics at the EP are predicted by the pure parasystole rules: at rational ratios one NIB prevails and the number and value of NIBs increase as we get tangentially closer to rational values. In contrast, in panel B, for cell #135, the distribution isn't similar: the highest probability NIBs are still present, but the overall pattern differs. From Fig. 9B, cell #135 has NIBs (1,4,6) which would correspond to the expected NIB values for  $\theta/T_{SN} = 0.6$  at  $R = 1.69$ . In Fig. 11C, we have the NIB evolution depending on  $R$  at cell #240 for  $\theta/T_{SN} = 0.6$  which corresponds better to Fig 11B. This further confirms the hypothesis that the NIB sequence in space corresponds to the NIB sequence as  $\theta$  increases.

#### 2.2.4: Comparing to real recordings

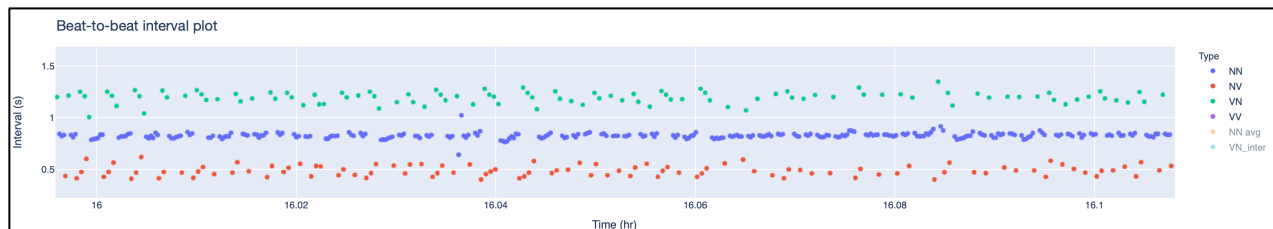


**Fig. 12:** Holter data recording from patient with frequent PVCs. Data from Icentia CardioSTAT, use of this data has been approved for research by the University of British Columbia Research Ethics Board. (Tom Bury, McGill 2020)

Now that we've established running simulations of pure parasystole in space, we can compare our results and predictions to real ECG recordings from patients. The CA model is an oversimplified model of parasystole, but it is the first step towards more realistic models. Despite this, we obtain interesting results and so, to what extent does what we see in this model applies to real life recordings? In Fig. 12, we have a Holter recording of a patient with parasystolic rhythms, suspected of having an ectopic pacemaker. In this recording, we have  $T_{SN} = 830\text{ms}$  and  $\theta$  is at most  $415\text{ms}$  (lowest coupling interval, NV, in the recording). The NIB values in this recording are 1, 4, 7 and 10 which does not contain a 'valid' triplet, but this is rather concealed trigeminy (3n-1). This does not match results from my model and it could be due to the fact that there is

modulation and entrainment in this recording. In contrast, other groups have found such patterns in modulated models (Moe et al 1977).

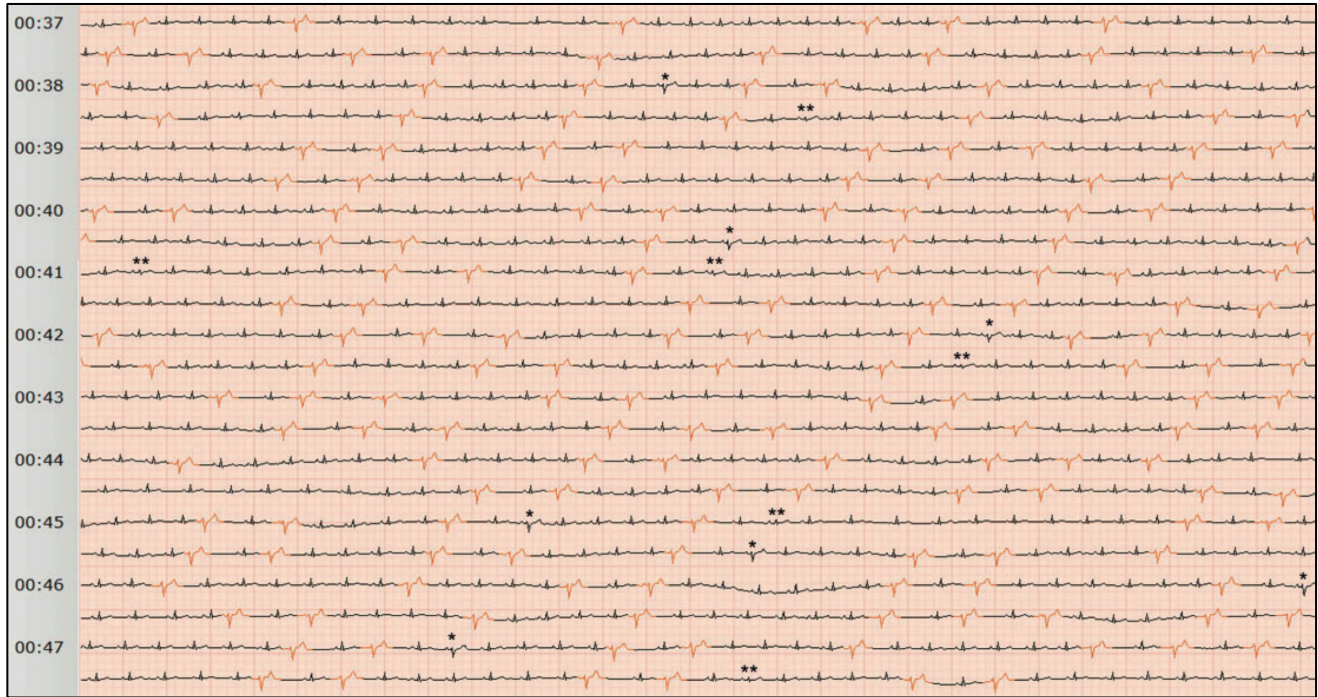


**Fig. 13:** Holter recording of patient diagnosed with ventricular parasystole (Steinfurt et al. 2018)

In Fig. 13, we have another Holter ECG recording of a patient diagnosed with ventricular parasystole (Steinfurt et al. 2018). Here, we have 2 NIBs triplets (1, 6, 8) and (1, 4, 6), the latter being the most dominant. From the Holter recording, we get  $T_{SN} = 800\text{ms}$ ,  $T_{EP} = 1800\text{ms}$  and  $\theta$  is at most  $400\text{ms}$ . At  $\theta = 375\text{ms}$ , our model expects NIB values of (1,4,6) in the region nearest to the EP and (1, 6, 8) in intermediate regions. Varying  $\theta$  and or R can help visualize possible dynamics to help define the actual parameters in the Holter data. In this case, our model's predictions seem to correlate with real recordings suggesting that in this patient we have little modulation, if not pure parasystole.

## CHAPTER 3: FITZHUGH-NAGUMO DIFFERENTIAL EQUATIONS MODEL

### 3.1: Methods

The Fitzhugh-Nagumo (FHN) model is a dynamical system that was initially built to model neural excitability (Fitzhugh, 1961) and the differential equations are as follows:

$$\begin{cases} \frac{dv}{dt} = v - \frac{v^3}{3} - r + I \\ \frac{dr}{dt} = \varepsilon(v + a - br) \end{cases} \quad (2)$$

with  $v$  the voltage variable,  $r$  the recovery variable,  $I$  the injected current and  $a$ ,  $b$  and  $\varepsilon$  are parameters that govern the solutions. The dynamics of the solutions can be observed in a phase-plane as in Fig. 14. In the phase-plane of this dynamical system, we have the cubic  $v$ -nullcline where solutions under the curve move to the right and solutions above the curve move to the left. Similarly, at the line  $r$ -nullcline, solutions on the left of it move down and solutions on the right move up. In Fig. 14A, when  $(a, b, \varepsilon) = (0.7, 0.7, 0.08)$ , the steady-state is a stable fixed point: for any initial conditions, the solution reach this point over time. In Fig. 14B, we have  $(a, b, \varepsilon) = (0.3, 0.5, 0.08)$  and in this case, there is a stable limit cycle. This limit-cycle results in AP formation and the ability of the system to fire AP from the parameters  $a$ ,  $b$  and  $\varepsilon$  will be referred to the intrinsic beating of the model, as opposed to the electrical stimulation with  $I$ . Parameter  $\varepsilon$  governs the shape of the APs and the duration of the refractory period ( $\theta$  is inversely related to  $\varepsilon$ ) and parameters  $a$  and  $b$  determine the firing frequency (the cycle length is directly related to  $a$  and  $b$ ). Thus, by adjusting these parameters the model can simulate excitable non-pacemaking and pacemaking tissue.

In order to model a line of 200 cells, the model is modified such that:

$$\begin{cases} \frac{dv}{dt} = v - \frac{v^3}{3} - r + I + D \frac{\partial^2 v}{\partial x^2} \\ \frac{dr}{dt} = \varepsilon(v + a - br) \end{cases} \quad (3)$$

where  $D \frac{\partial^2 v}{\partial x^2}$  is the diffusion term that connects the cells together. When taking the diffusion coefficient  $D = 0.05 \text{ cell}^2/\text{dt}$ , it takes 90 time-steps (at  $\varepsilon = 0.01$ ) for the pulse to travel 200 cells. Using the same physiological parameters as in the CA model, CV (in ventricles) = 50cm/s and length of heart of 12cm, we have in our model that  $1dt = 2.35\text{ms}$  and  $1dx = 0.6\text{mm}$ . The SN and

EP pacemakers are located at each end of the strip of 200 cells and the firing frequency of either pacemaker can be controlled with  $(a, b, \varepsilon)$  and/or driven with fixed stimulation by changing  $I$ .

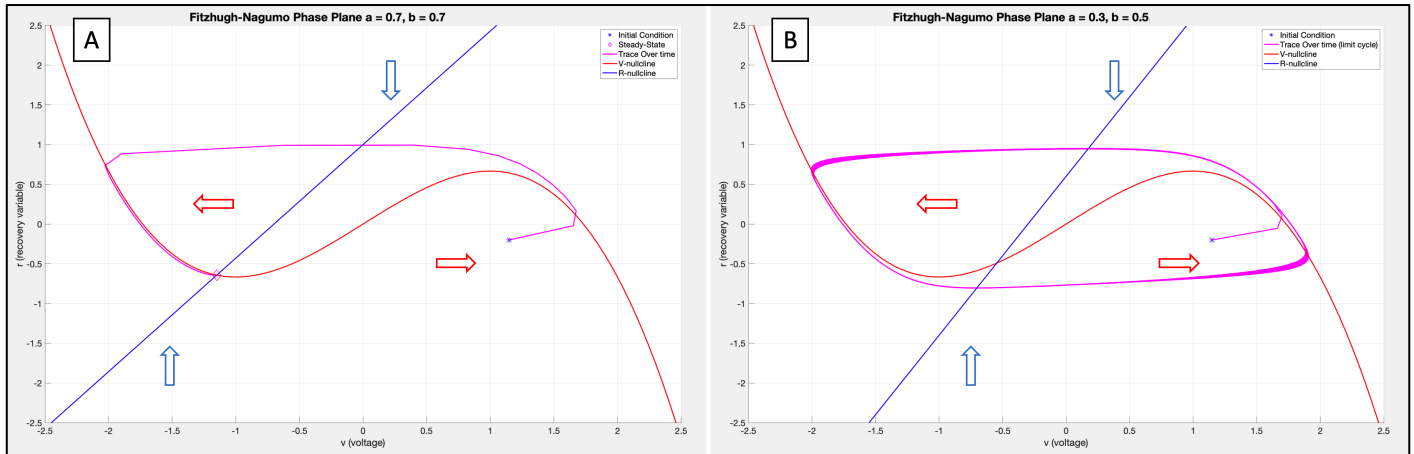


**Fig 14:** FHN model. Phase-plane of the FHN model. A)  $(a, b, \varepsilon, I) = (0.7, 0.7, 0.08, 0)$ . B)  $(a, b, \varepsilon, I) = (0.3, 0.5, 0.08, 0)$

The simulations are run using the programming software MATLAB R2019a. The differential equations are integrated with MATLAB's function ODE45, which is based on the Dormand-Prince method, a numerical analysis that utilizes the 4<sup>th</sup> and 5<sup>th</sup> order of the Runge-Kutta method (Dormand & Prince, 1980).

3.2: Results

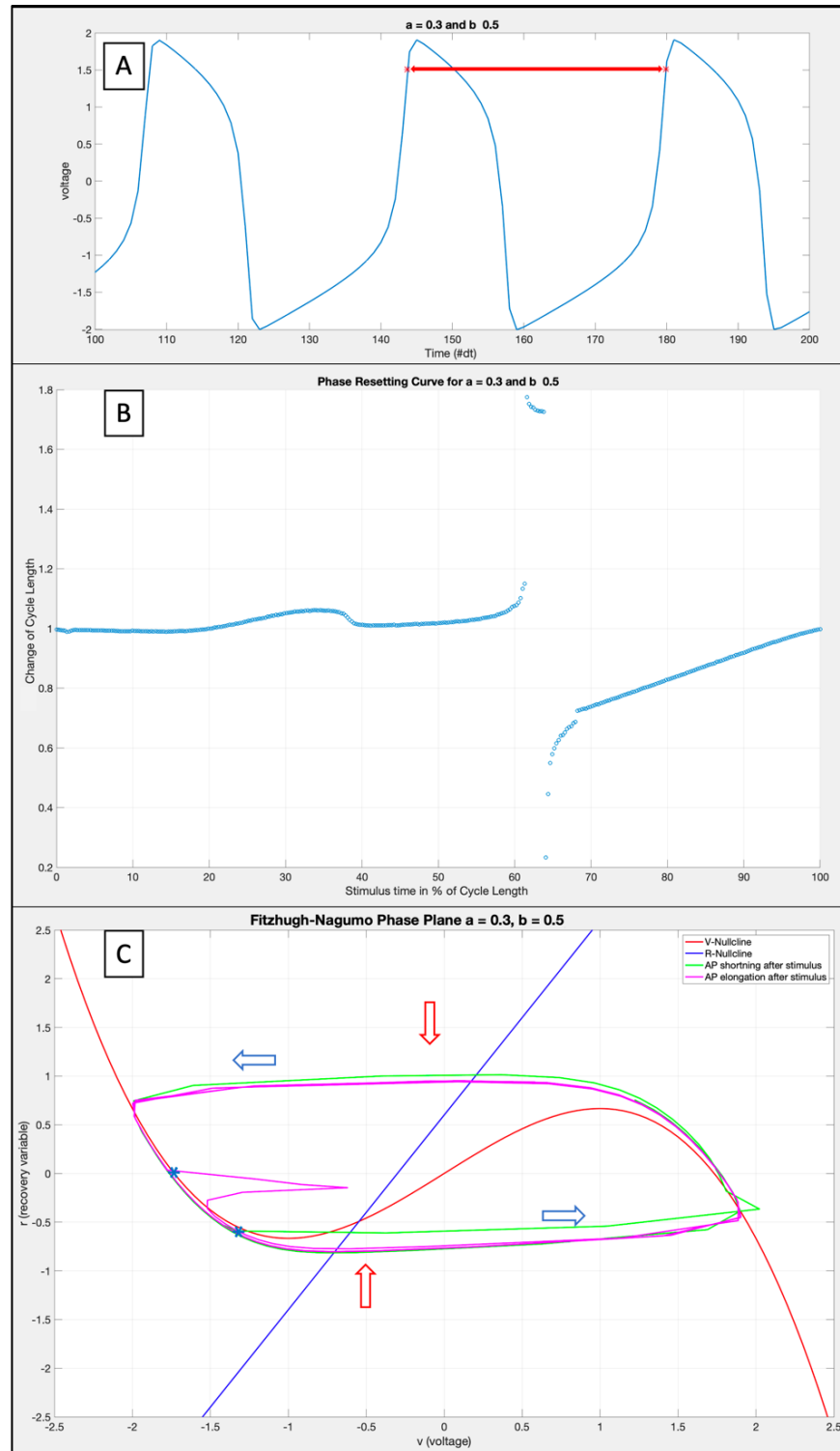


**Fig. 15:** FHN model, phase-resetting. A) AP trace, red arrow represents the region stimuli will be applied to for the PRC. B) Phase-Resetting curve C) Phase-plane when phase-resetting: pink = AP delay, green = AP shortening.

An important aspect of the FHN model is that as a model of an oscillator, it can yield phase-resetting. When delivering an electrical impulse at different times along the cycle (Fig. 15A), we obtain the PRC in Fig 15B. As earlier models have shown, there is an increase of the cycle length when the stimulus is early in the cycle and a shortening when the stimulus is late in the cycle. This phenomenon is explained by the phase-plane in Fig 15C: two stimuli (the blue asterisks) applied at different times in the cycle resulted in cycle length lengthening (pink trace) and cycle length shortening (green trace). The cycle length will be reduced if the strength and timing of the impulse allows the trace to cross the  $r$ -nullcline (trigger an AP), otherwise, the voltage will come back down to the limit cycle, resulting in a greater cycle length.

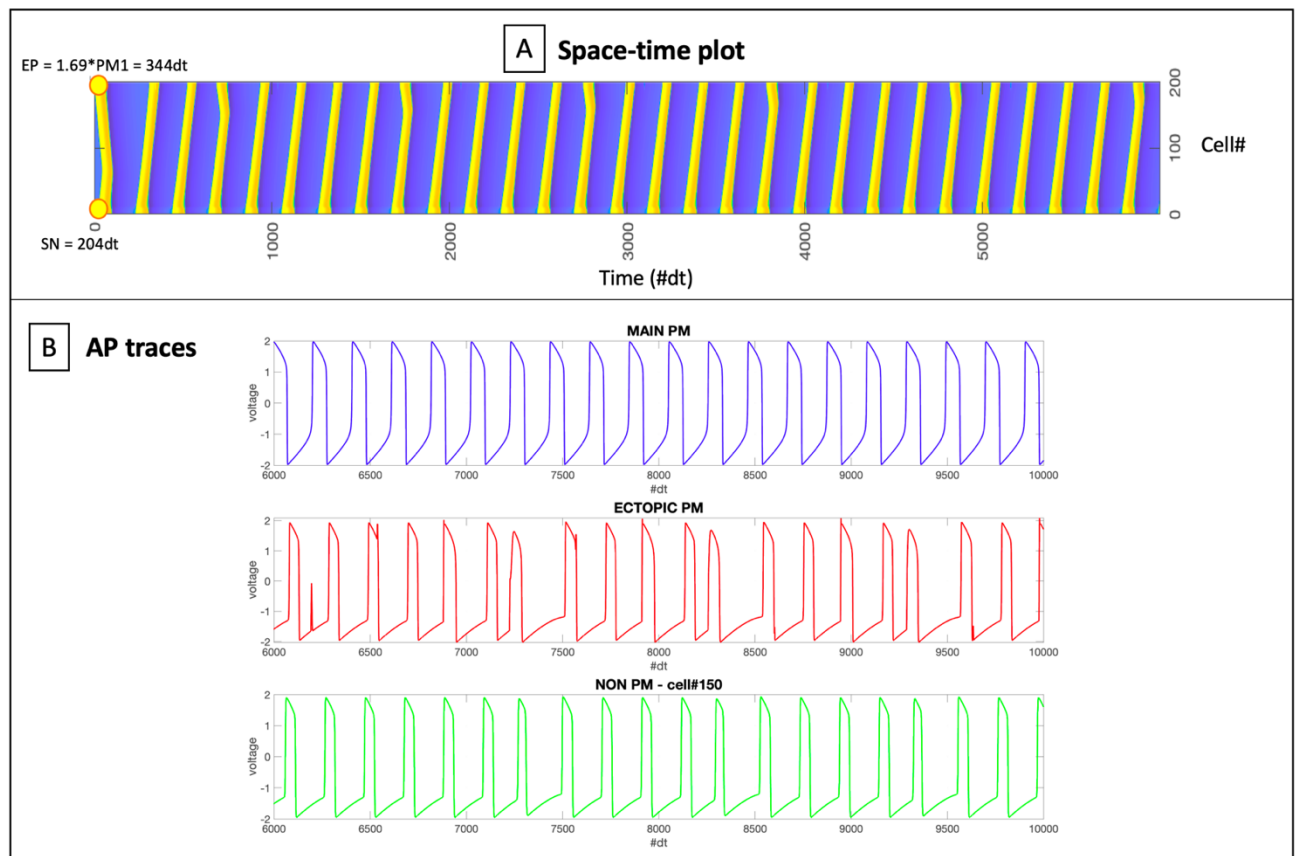


**Fig. 16:** FHN model. A) Space-time plot with  $(a, b, \varepsilon, I) = (0.7, 0.7, 0.01, 0)$  for excitable cells,  $(a, b, \varepsilon, I) = (0.3, 0.5, 0.01, 0)$  at SN (cell #1) for  $T_{SN} = 204dt$ ,  $(a, b, \varepsilon, I) = (0.7, 0.7, 0.01, 1)$  at EP (cell #200) for  $T_{EP}/T_{SN} = 1.69$  and  $\theta = 92$ . B) AP traces at SN, EP and cell #150

With parameters  $(a, b, \varepsilon) = (0.7, 0.7, 0.01)$  for excitable cells,  $(a, b, \varepsilon) = (0.3, 0.5, 0.01)$  at SN (cell #1) for  $T_{SN} = 204.14dt$ ,  $I = 1$  at EP (cell #200) for  $T_{EP}/T_{SN} = 1.69$  and  $\theta/T_{SN} = 0.45$ , we

obtain the space-time plot in Fig. 16A. Once again, we can see that an ectopic pulse occasionally manages to escape SN's refractory period and depolarize cells in its vicinity. In Fig. 16B, we have AP traces for different cells: the main PM (SN) fires regularly whereas in the EP trace, we can see that point stimuli occur at different point in the SN cycle, where stimuli are sometimes being silenced, and at other times they are expressed. In the bottom panel, we have the AP trace of cell #150 where we can observe that the activity of both pacemakers results in varying cycle lengths in the excitable tissue. Fig 17A and 17B show the cycle length variation for cells #150 and #175 respectively. As expected, there is more variation in the region closer to the EP (cell #175).

As just described, the cycle lengths and number of EP beats varies with space. To compare this with the results from the CA model, I simulated a line of 200 excitable cells where SN and EP are electrically stimulated at fixed frequencies (no phase-resetting possible). To make this more comparable to the CA model, as  $1dt = 2.35ms$ , I set  $T_{SN} = 356dt = 836.6ms$  and  $\theta/T_{SN} = 0.37$ . Running simulations for different values of  $T_{EP}/T_{SN}$  and recording the NIB values in space, I obtain Table 1. As before, in regions near EP, the NIBs follow the predictions of pure parasystole earlier described. Further from the ectopic focus, the NIBs change in the same manner they would if the refractory period is increased (Fig. 5). As in the CA model, we can write an equation to determine the furthest reach of the EP wave:

$$x = CV \left[ \frac{1}{2}(2T_N + \theta - T_{SN}) \right] \quad (4)$$

where  $x$  is the number of cells from SN,  $CV$  is the conduction velocity,  $T_N$  is the time to go across all cells from SN to EP,  $\theta$  is the refractory period (in #dt) and  $T_{SN}$  is the period of SN (in #dt). The EP wave will reach SN if  $2T_N + \theta < T_{SN}$ , Recall that when using  $(a, b, \varepsilon)$  to pace SN, there is a possibility of phase resetting and so, the FHN model could potentially be a model for modulated parasystole. However, with intrinsic beating the refractory period  $\theta$  is too large to allow for  $x < 0$ , and so in this case, the EP wave never reaches SN and no phase resetting is possible. For instance, at  $(a, b, \varepsilon) = (0.3, 0.5, 0.01)$  we have  $T_{SN} = 205.74dt$  and  $\theta = 131.90dt$  ( $\theta/T_{SN} > 0.5!$ ) and the high  $\theta/T_{SN}$  seems to be sustained at all pacing  $(a, b, \varepsilon)$  setting and so, some modifications to the model would be necessary to allow the possibility of phase resetting in the parasystole FHN model. Thus, if the EP wave never reaches SN phase resetting is not possible and the model resembles that of pure parasystole

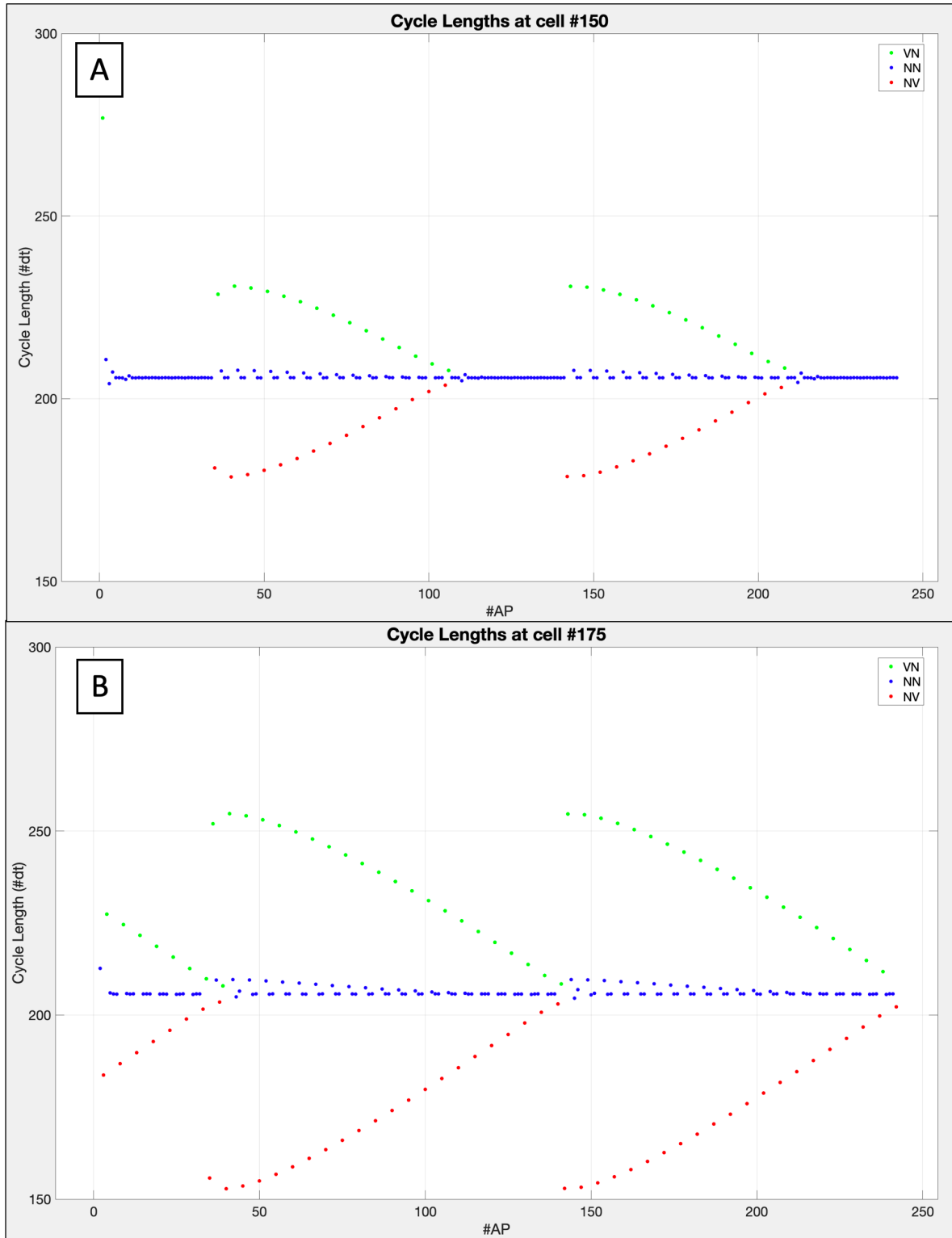


**Fig. 17:** FHN model. Cycle length plots from the data in Fig. 17. A) Cell # 150. B) Cell #175

**Table 1:** FHN model. NIB values in pure parasystole model.  $T_{SN} = 356dt = 836.6ms$  and  $\theta/T_{SN} = 0.37$ .

$T_{EP}/T_{SN}$	1.213	1.376	1.438	1.542	1.691	1.744	1.811	1.947	2.342	3.739
Cell # 10	0, 4, 5	2, 3, 6	2, 6, 9	2, 10, 13	4, 6, 11	1, 4, 6	1, 6, 8	1, 26, 28	4, 6, 32	3, 10, 14
Cell # 50	0, 4, 5	2, 3, 6	2, 3, 6	2, 7, 10	1, 4, 6	1, 4, 6	1, 6, 8	1, 24, 26	1, 4, 6	3, 10, 14
Cell # 75	0, 3, 4	0, 2, 3	2, 3, 6	2, 4, 7	1, 2, 4	1, 4, 6	1, 6, 8	1, 22, 24	1, 4, 6	3, 10, 14
Cell # 100	0, 3, 4	0, 2, 3	0, 2, 3	2, 4	1, 2, 4	1, 4, 6	1, 4, 6	1, 20, 22	1, 4, 6	3, 10
Cell # 125	0, 3, 4	0, 2, 3	0, 2, 3	1, 2, 4	1, 2, 4	1, 2, 4	1, 4, 6	1, 18, 20	1, 4, 6	3, 6, 10
Cell # 150	0, 3, 4	0, 2, 3	0, 2, 3	0, 1, 2	1, 2, 4	1, 2, 4	1, 4, 6	1, 16, 18	1, 4, 6	3, 6, 10
Cell # 190	0, 2, 3	0, 1, 2	0, 1, 2	0, 1, 2	1, 2, 4	1, 2, 4	1, 2, 4	1, 14	1, 4, 6	3, 6, 10

The range of  $\theta$  possible from  $(a, b, \varepsilon)$  is relatively narrow as mentioned. Another possibility for studying phase resetting in the parasystole FHN model would be to reduce the distance between SN and EP enough such that  $2T_N + \theta < T_{SN}$ . This is the case when we have  $N = 60$  ( $T_N = 29dt$ ) and at this distance, the EP wave can reach SN and cause phase resetting. In Fig. 18 we compare the cycle lengths plots at cell #45 when there is no phase resetting (panel A) and when there is (panel B). In Fig. 18A, we stimulate SN with  $I = 1$  at a fixed cycle length of  $204dt$  and  $T_{EP}/T_{SN} = 1.69$ . In Fig 18B, we have at SN  $(a, b, \varepsilon) = (0.3, 0.5, 0.01)$  for  $T_{SN} = 204.14dt$  and  $T_{EP}/T_{SN} = 1.69$ . From Fig. 18, we can see that phase-resetting affects the duration of cycle lengths (mostly VN) and the logical pattern seen in the absence of phase-resetting seems to be lost. Recall that in the pure parasystole model, we have  $NV + VN = 2NN$ , in Fig. 19 we compare the sum of NV and VN from the data in Fig. 18. Without phase-resetting, the sum of NV and VN is of about  $408dt$  as expected. In phase-resetting however, we can see that this is not always the case, the sum of NV and VN fluctuates, often below the expected value. From the PRC curve of our model (Fig. 15B), we can see that the SN pacemaker has a very short region of cycle length elongation and large region of cycle length shortening: the SN seems to be more often entrained and this could explain the reduction of  $NV+VN$  in phase-resetting experiments.

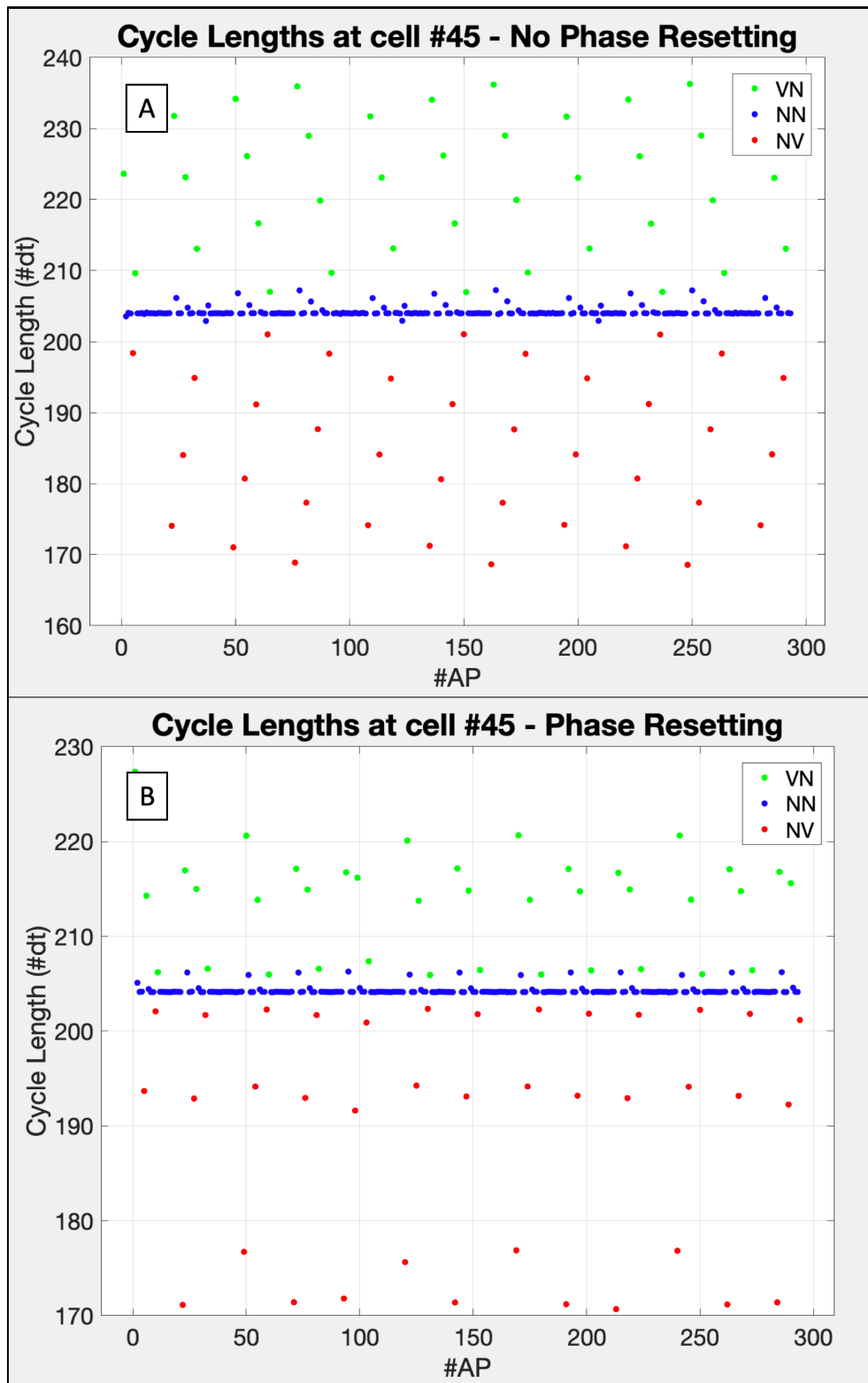


**Fig 18:** FHN model.  $N = 60$ . A) No phase resetting: at SN,  $(a, b, \varepsilon, I) = (0.7, 0.7, 0.01, 1)$ ,  $T_{SN} = 204dt$  and  $T_{EP}/T_{SN} = 1.69$ . B) Phase resetting: at SN,  $(a, b, \varepsilon, I) = (0.3, 0.5, 0.01, 0)$ ,  $T_{SN} = 204.14dt$  and  $T_{EP}/T_{SN} = 1.69$ .

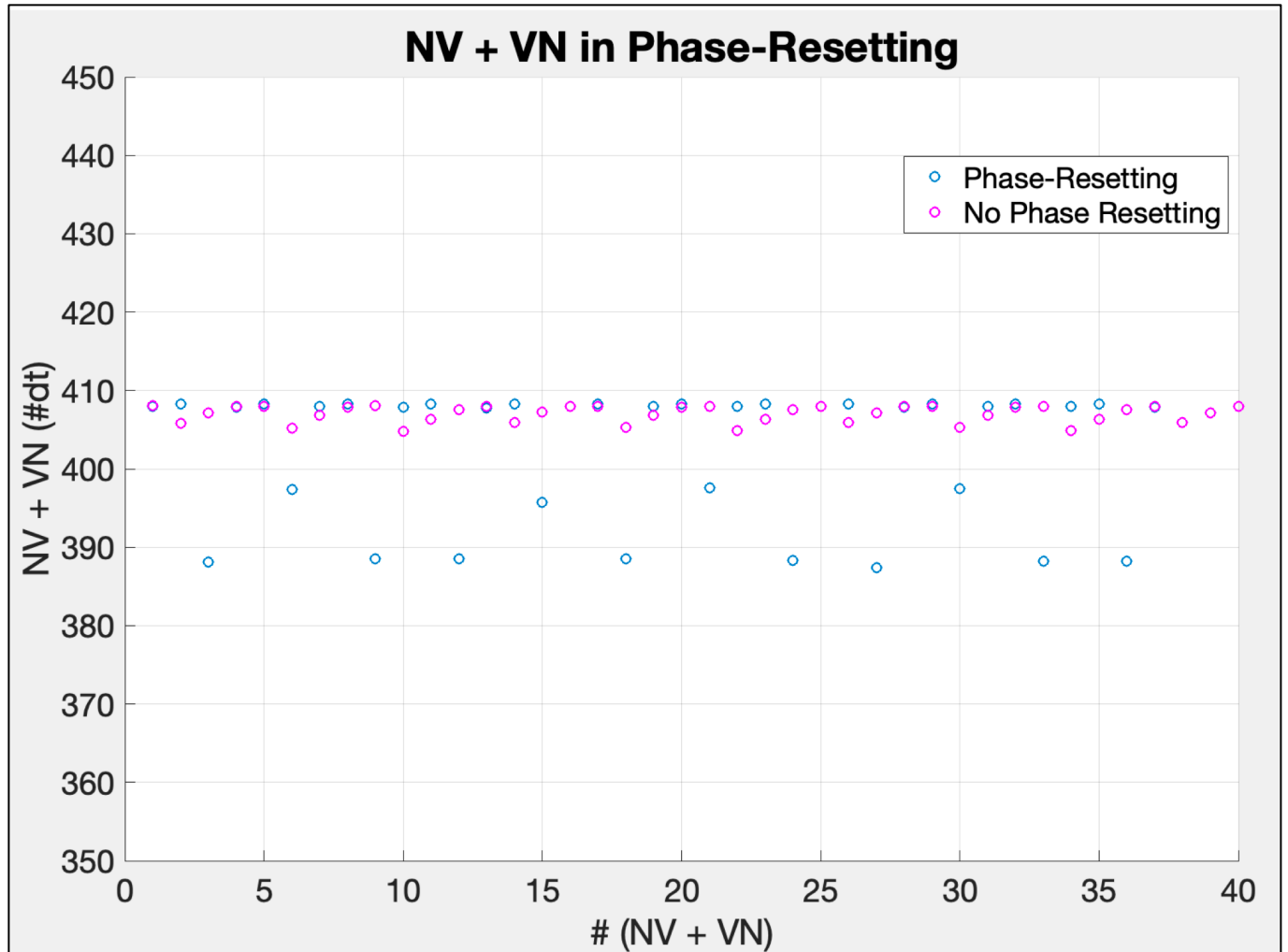


Fig. 19: FHN model. Comparison of  $NV+VN$  interval with or without phase-resetting, using data from Fig. 19

## CHAPTER 4: DISCUSSION

### 4.1: Limitations

In this project, I have built the first models of parasystole including the excitable media between the pacemakers. There are however some limitations in the models that could potentially affect the results.

Firstly, the CA model of parasystole is discrete in space and in time. In real life however, AP propagation is not an on/off phenomenon but there is rather a continuous change, both in time and in space, in voltage and ionic concentrations in cardiac tissue. The discretization of the CA model can skew the results, omitting some finer details of the dynamics.

Secondly, the FHN model was built to represent neuronal activity but neuronal dynamics differ from cardiac dynamics. In neurons, APs are short in duration and do not have a plateau phase. This difference in AP formation can undermine the predictions made for the dynamics seen in the model of parasystole.

Thirdly, both models discussed here are one-dimensional. In cardiac tissue, the waves interact in three-dimensional excitable tissue and so, real-life dynamics are likely far more complex than in our one-dimensional models.

Lastly, we show that there is an evolution of NIB in the tissue separating the pacemakers. How this translates into the ECG still remains a mystery. Most of the time, in the whole heart PVCs propagate through the whole ventricles. When both the SA node and the ectopic pacemaker fire at once we obtain fusion beats, of intermediate morphology (i.e.: there aren't normal APs in regions near the SA node and PVCs near the ectopic focus). So, it is unlikely that we would see regions with different NIBs in the real heart, as we do in the simulations. I hypothesize that the dominant pattern, depending on the distance between the pacemakers, would be expressed in the ECG. This however remains an open question and requires greater analysis.

### 4.2: Conclusions

The models I've built here, in addition to including space, have some notable differences from mathematical models previously described. Without space, older models had to impose compensatory pauses when the ectopic pacemaker fires and fusion beats when both pacemakers

fired at almost the same time. In my models however, compensatory pauses occur because after an ectopic beat, the ‘tissue’ is refractory and cannot propagate another AP from SN. This is similar to what would happen in the real heart. Interestingly because compensatory pauses aren’t imposed at every ectopic beat, my simulations also allow for the possibility of interpolated beats. Interpolated beats are only possible if  $T_{SN} > 2(T_N + \theta)$ , where  $T_{SN}$  is the period of the SA node,  $T_N$  is the time the AP takes to travel through the whole tissue and  $\theta$  is the refractory period. They cause intermediate NIB values that do not follow the rules of pure parasystole previously described (Glass et al. 1986), recall that compensatory pauses were imposed after every ectopic beat in this paper. Accordingly, compensatory pauses, interpolated beats and fusion beats need not be added in my simulations as they are naturally present in a biological parasystole model with excitable cells between pacemakers.

With these models, I have verified previous predictions of parasystole and have noted new observations that have not been described before. In both CA and FHN models, when modeling pure parasystole without interpolated beats ( $T_{SN} < 2(T_N + \theta)$ ), we have:

- 1) At any point in space, the first 3 NIB rules from Glass et al. 1986 are upheld (a NIB triplet such that only one of these values is odd and the sum of the two smallest is one less the largest)
- 2) The NIB triplet evolution as we move in space, away from EP, matches the NIB triplet sequence as we increase the refractory period in a dimensionless model
- 3) For two pacemakers SN and EP separated by a line of N cells, we can calculate the maximum propagation distance of the EP wave by using the equation (4):  $x = CV \left[ \frac{1}{2}(2T_N + \theta - T_{SN}) \right]$ , where  $x$  is the distance from SN,  $CV$  is the conduction velocity,  $T_N$  is the time an AP takes to get across all cells from SN to EP,  $\theta$  is the refractory period and  $T_{SN}$  is the firing period for SN. Note that the largest zone that the EP can depolarize is independent from its cycle length.

Next, the FHN model also allows for phase resetting and can be used to simulate modulated parasystole. In our preliminary simulations, SN is often entrained by the EP, as confirmed by its PRC’s morphology.

### 4.3: Future directions

The models of parasystole described in this project successfully introduced a spatial dimension to the simulations. Now, several directions can be taken in order to better comprehend the dynamics involved in pure and modulated parasystole.

The FHN model is a very simple model of neural activity and in order to make accurate conclusions for the real heart, the model needs to be modified. There exist variations of the FHN model for cardiac tissue such as the Aliev-Panfilov model (Aliev and Panfilov 1996). In this adaptation, the authors have built a model of cardiac excitation where the AP morphology and restitution curve match that of cardiac tissue. Using such a model of cardiac excitation instead of the normal FHN model will make our simulations of parasystole more reliable.

Next, we can set up CA model in a two-dimensional lattice where waves can propagate in any direction (not in two directions as it does in the one-dimensional model). The possibility of more complex dynamics in 2D (re-entry, spirals...) can bring a greater level of understanding of how parasystolic dynamics are linked to more complex arrhythmias.

We can also build experimental models of parasystole in order to validate our theoretical models, as was done in several key early studies in this field (Scherf & Chick, 1951 and Jalife & Moe, 1976). A promising direction is to use optogenetic techniques to generate two interacting pacemakers where the distance between the pacemakers and their relative periods can be adjusted. This would allow us to observe how two interacting pacing sites separated by excitable tissue interact. We performed a small number of proof-of-principle experiments using techniques described in Burton et. al, 2015 to illustrate the feasibility of this optogenetic approach (Burton et al. 2015). We generated cardiac monolayers of neonatal murine myocytes and transfected them with a viral construct that caused the cells to express a light sensitive channel (channelrhodopsin-2, ChR2). The monolayers were stimulated using blue patterned light from a projector that was programmed to illuminate two locations on the monolayer with brief pulses of different user-defined periods. Wave propagation is visualized using a dye-free imaging modality which

translates local cell contraction to intensity changes in a recorded video. Our preliminary recordings are shown in Fig. 20.

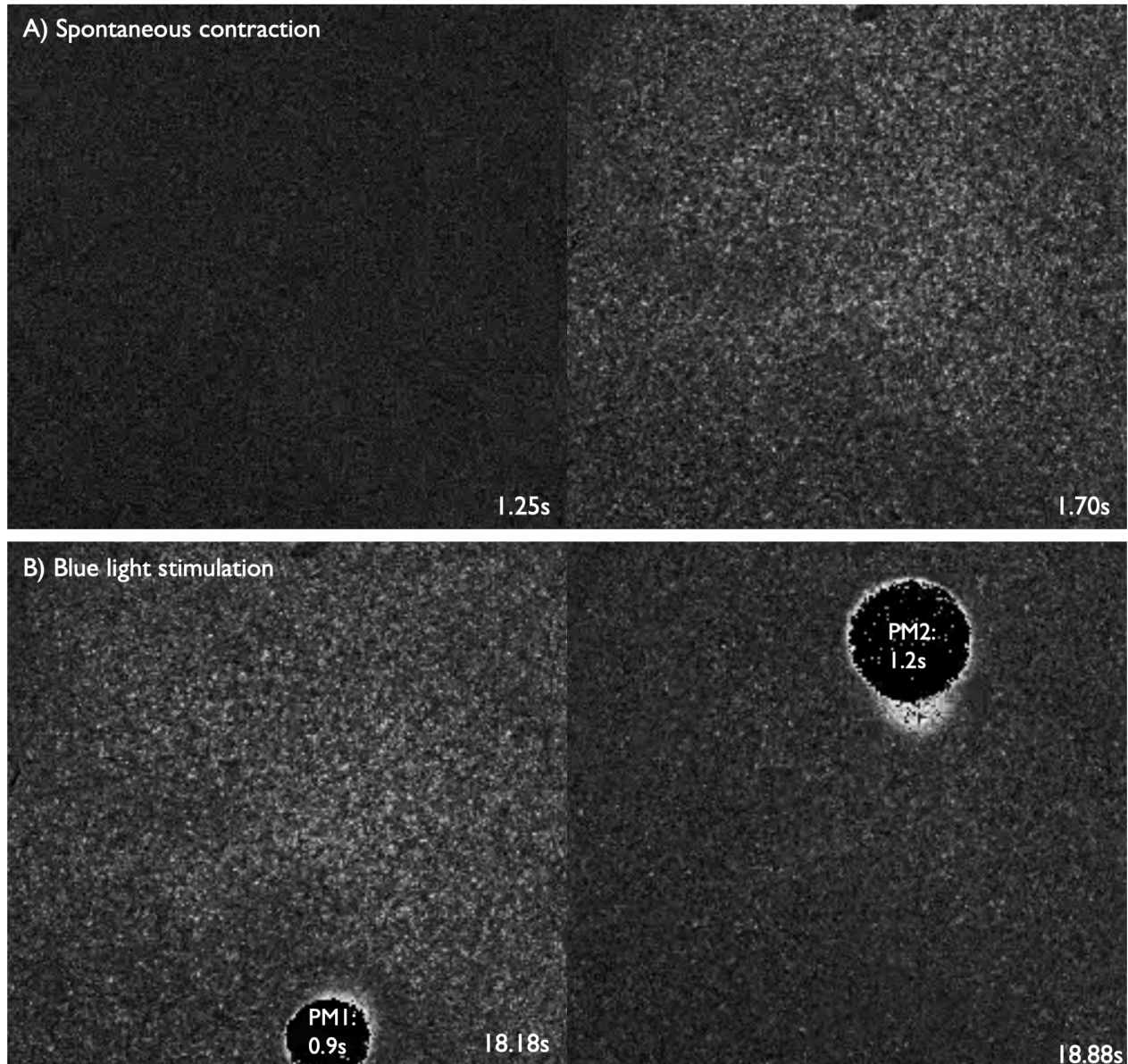


**Fig. 20:** Preliminary results of the cardiomyocyte monolayer: white represents contracting cells. A) Spontaneous contraction of the monolayer B) Stimulating two pacemakers with blue light: PM1 is stimulated every 0.9s and PM2 every 1.2s.

Our preliminary results in Fig. 20 allows us to see what could be done in an experimental context if these protocols were developed further. In Fig. 20A we see that the monolayer, as expected from previous studies using this preparation (Burton et al, 2015), has an intrinsic

capability to contract at its own pace. We next stimulated two pacemaker regions using blue light. One pacemaker at the bottom with a cycle length of 0.9s and one at the top with a cycle length of 1.2s. In the 25 seconds recording, captured in Fig. 20B, the faster (bottom) pacemaker is dominant and the slow pacemaker (top) is silenced as it fires in the refractory period of the tissue. This confirms that the experimental monolayer can be stimulated with blue light, but a stimulus will not propagate if the tissue is refractory. While these experiments show that it is feasible to use optogenetics to generate parasystolic rhythms, there are several limitations that need to be addressed. The first is the 2D flat shape of the monolayer, as opposed to the complex 3D morphology of a real heart. And the second is the homogeneity of the tissue, lacking the zone of depressed conduction that protects the ectopic pacemaker. Entry-block could be modeled in the monolayer setting either by using rings of dim light (functional heterogeneity) or by changing the shape of the monolayer (structural heterogeneity), note however that these are suggestions and have not been tested yet.

We could also use a whole-heart preparation to do similar experiments. The Langendorff heart preparation allow for studies on the ex-vivo living whole heart while it is suspended in an apparatus that perfuses it with a physiological solution of salts and sugars (as done by Wengrowski et al. 2015, Bruegmann et al. 2016, Watanabe et al. 2017 and Scardigli et al.2018). The heart can either be transfected with channelrhodopsin-2, or it can be obtained from a transgenic mouse expressing the opsin in the heart. As in the cardiomyocyte monolayer, we can stimulate a pacemaking region in the ventricles and at the SA node to obtain a three-dimensional experimental model of parasystole. Optogenetic stimulation is potentially better than electrical stimulation for a number of reasons. First, using light we can easily change the geometry of the pacemaking site and use this to model unidirectional block: note however that how this could be done is still unclear. Next, we can change the period of pacing of each pacemaker and the distance between them more readily than with electrical stimulations. And finally, optogenetics can allow us to model modulated parasystole in excitable tissue by creating a resettable pacemaker through constantly illuminating a region to depolarize the ventricles.

ECG recordings from experiments in whole hearts and monolayers would allow us to better understand how the spatial effects we see in the CA and FHN models would translate to the ECG

recordings of parasystole in humans. This would in turn shed some light on unexplained NIB patterns in some patients. In addition, the three-dimensional experimental model of parasystole can ultimately be used to build an accurate three-dimensional simulation of parasystole. In this simulation, parasystolic parameters (SA node cycle length, EP cycle length, refractory period, degree of modulation...) could be varied and studied more efficiently than in experimental models.

## REFERENCES

1. Acharya, U. R., Joseph, K. P., Kannathal, N., Lim, C. M., & Suri, J. S. (2006). Heart rate variability: a review. *Medical and biological engineering and computing*, 44(12), 1031-1051.
2. Alanís, J., González, H., & López, E. (1958). The electrical activity of the bundle of His. *The Journal of physiology*, 142(1), 127-140.
3. AlGhatrif, M., & Lindsay, J. (2012). A brief review: history to understand fundamentals of electrocardiography. *Journal of community hospital internal medicine perspectives*, 2(1), 14383.
4. Aliev, R.R. and Panfilov, A.V. (1996). A simple two-variable model of cardiac excitation. *Chaos, Solitons & Fractals*, 7(3), pp.293-301.
5. Antzelevitch, C., Bernstein, M. J., Feldman, H. N., & Moe, G. K. (1983). Parasyctole, reentry, and tachycardia: a canine preparation of cardiac arrhythmias occurring across inexcitable segments of tissue. *Circulation*, 68(5), 1101-1115.
6. Antzelevitch, C., Jalife, J., & Moe, G. K. (1980). Characteristics of reflection as a mechanism of reentrant arrhythmias and its relationship to parasyctole. *Circulation*, 61(1), 182-191.
7. Baldizhar, A., Manuylova, E., Marchenko, R., Kryvalap, Y., & Carey, M. G. (2016). Ventricular tachycardias: characteristics and management. *Critical Care Nursing Clinics*, 28(3), 317-329.
8. Baman, T. S., Lange, D. C., Ilg, K. J., Gupta, S. K., Liu, T. Y., Alguire, C., & Pelosi Jr, F. (2010). Relationship between burden of premature ventricular complexes and left ventricular function. *Heart Rhythm*, 7(7), 865-869.
9. Bean, B. P. (2007). The action potential in mammalian central neurons. *Nature Reviews Neuroscience*, 8(6), 451-465.
10. Bers, D. M. (2002). Cardiac excitation–contraction coupling. *Nature*, 415(6868), 198-205.
11. Bruegmann, T., Boyle, P. M., Vogt, C. C., Karathanos, T. V., Arevalo, H. J., Fleischmann, B. K., ... & Sasse, P. (2016). Optogenetic defibrillation terminates ventricular arrhythmia in mouse hearts and human simulations. *The Journal of clinical investigation*, 126(10), 3894-3904.
12. Bub, G., Glass, L., Publicover, N.G. and Shrier, A., (1998). Bursting calcium rotors in cultured cardiac myocyte monolayers. *Proceedings of the National Academy of Sciences*, 95(17), pp.10283-10287.
13. Burton, R. A., Klimas, A., Ambrosi, C. M., Tomek, J., Corbett, A., Entcheva, E., & Bub, G. (2015). Optical control of excitation waves in cardiac tissue. *Nature photonics*, 9(12), 813-816.
14. Dampney, R. A. (1994). Functional organization of central pathways regulating the cardiovascular system. *Physiological reviews*, 74(2), 323-364.
15. de Lange, E., Xie, Y. and Qu, Z., (2012). Synchronization of early afterdepolarizations and arrhythmogenesis in heterogeneous cardiac tissue models. *Biophysical journal*, 103(2), pp.365-373.
16. Dormand, J.R. and Prince, P.J., (1980). A family of embedded Runge-Kutta formulae. *Journal of computational and applied mathematics*, 6(1), pp.19-26.

17. Euler, D. E. (1999). Cardiac alternans: mechanisms and pathophysiological significance. *Cardiovascular research*, 42(3), 583-590.
18. FitzHugh, R., (1961). Impulses and physiological states in theoretical models of nerve membrane. *Biophysical journal*, 1(6), p.445.
19. Fleming, G. B. (1912). Triple rhythm of the heart due to ventricular extrasystoles. *QJ Med*, 5, 318-326.
20. Gardner, R. T., Ripplinger, C. M., Myles, R. C., & Habecker, B. A. (2016). Molecular mechanisms of sympathetic remodeling and arrhythmias. *Circulation: Arrhythmia and Electrophysiology*, 9(2), e001359.
21. Glass, L., Goldberger, A. L., & Belair, J. (1986). Dynamics of pure parasystole. *American Journal of Physiology-Heart and Circulatory Physiology*, 251(4), H841-H847.
22. Gordan, R., Gwathmey, J. K., & Xie, L. H. (2015). Autonomic and endocrine control of cardiovascular function. *World journal of cardiology*, 7(4), 204.
23. Guevara, M. R., Alonso, F., Jeandupeux, D., & Van Ginneken, A. C. (1989). Alternans in periodically stimulated isolated ventricular myocytes: Experiment and model. In *Cell to Cell Signalling* (pp. 551-563). Academic Press.
24. Hoshino, K., Ikeda, N., Miyahara, H., & Sato, T. (1989b). Reentrant arrhythmias generated by a computer-based model of the modulated parasystole in an open-chest dog. *Japanese heart journal*, 30(6), 885-894.
25. Hoshino, K., Ikeda, N., Tanakadate, A., & Miyahara, H. (1989a). A computer-based model of parasystolic activity modulated by ventricular activation in the open-chest dog. *Journal of electrocardiology*, 22(4), 277-283.
26. Ikeda, N., Tsuruta, H., & Sato, T. (1981). Difference equation model of the entrainment of myocardial pacemaker cells based on the phase response curve. *Biological Cybernetics*, 42(2), 117-128.
27. Ikeda, N., Yoshizawa, S., & Sato, T. (1983). Difference equation model of ventricular parasystole as an interaction between cardiac pacemakers based on the phase response curve. *Journal of theoretical biology*, 103(3), 439-465.
28. Jalife, J., & Moe, G. K. (1976). Effect of electrotonic potentials on pacemaker activity of canine Purkinje fibers in relation to parasystole. *Circulation Research*, 39(6), 801-808.
29. Jalife, J., Michaels, D. C., & Langendorf, R. (1986). Modulated parasystole originating in the sinoatrial node. *Circulation*, 74(5), 945-954.
30. Kervancıoğlu, M., Özbağ, D., Kervancıoğlu, P., Hatipoğlu, E. S., Kiliç, M., Yılmaz, F., & Deniz, M. (2003). Echocardiographic and morphologic examination of left ventricular false tendons in human and animal hearts. *Clinical Anatomy: The Official Journal of the American Association of Clinical Anatomists and the British Association of Clinical Anatomists*, 16(5), 389-395.
31. Kléber, A. G., & Rudy, Y. (2004). Basic mechanisms of cardiac impulse propagation and associated arrhythmias. *Physiological reviews*, 84(2), 431-488.
32. Lin, C. Y., Lin, Y. J., Chen, Y. Y., Chang, S. L., Lo, L. W., Chao, T. F., ... & Tuan, T. C. (2015). Prognostic significance of premature atrial complexes burden in prediction of long-term outcome. *Journal of the American Heart Association*, 4(9), e002192.
33. Loskutov, A., Rybalko, S., & Zhuchkova, E. (2004). Model of cardiac tissue as a conductive system with interacting pacemakers and refractory time. *International Journal of Bifurcation and Chaos*, 14(07), 2457-2466.

34. Lucas, K. (1912). On a mechanical method of correcting photographic records obtained from the capillary electrometer. *The Journal of physiology*, 44(3), 225.
35. Malik, M. (1996). Heart rate variability: Standards of measurement, physiological interpretation, and clinical use: Task force of the European Society of Cardiology and the North American Society for Pacing and Electrophysiology. *Annals of Noninvasive Electrocardiology*, 1(2), 151-181.
36. Manas & Sumit Verma. (2019). Current Management of Premature Ventricular Contractions. A Review. *EC Cardiology* 6(11): 83-89.
37. Médigue, C., Girard, A., Laude, D., Monti, A., Wargon, M., & Elghozi, J. L. (2001). Relationship between pulse interval and respiratory sinus arrhythmia: a time-and frequency-domain analysis of the effects of atropine. *Pflügers Archiv*, 441(5), 650-655.
38. Moe, G. K., Jalife, J. O. S. E., Mueller, W. J., & Moe, B. R. U. C. E. (1977). A mathematical model of parasystole and its application to clinical arrhythmias. *Circulation*, 56(6), 968-979.
39. Mohammadi, S., Hedjazi, A., Sajjadian, M., Ghoroubi, N., Mohammadi, M. and Erfani, S., (2016). Study of the normal heart size in Northwest part of Iranian population: a cadaveric study. *Journal of cardiovascular and thoracic research*, 8(3), p.119.
40. Munger, T. M., Wu, L.Q., Shen, W. K. (2014). Atrial fibrillation. *Journal of Biomedical Research*. 28(1), 1-17.
41. NHLIB. (2011). Types of Arrhythmia. *NHLIB*. Retrieved June 2020 from <https://web.archive.org/web/20150607165144/http://www.nhlbi.nih.gov/health/health-topics/topics/arr/types>
42. Pick, A. (1953). Parasystole. *Circulation*, 8(2), 243-252.
43. Saoudi, N., Letac, B., & Castellanos, A. (1995). An electronic model for evaluating the dynamics of perfect pure parasystole in the human heart. *The American journal of cardiology*, 75(10), 739-742.
44. Scardigli, M., Müllenbroich, C., Margoni, E., Cannazzaro, S., Crocini, C., Ferrantini, C., ... & Bocchi, L. (2018). Real-time optical manipulation of cardiac conduction in intact hearts. *The Journal of physiology*, 596(17), 3841-3858.
45. Scarle, S. and Clayton, R.H., (2009). Early afterdepolarisations and ventricular arrhythmias in cardiac tissue: a computational study. *Medical & biological engineering & computing*, 47(3), p.291.
46. Scherf, D., & Chick, F. B. (1951). Experimental parasystole. *American Heart Journal*, 42(2), 212-225.
47. Setiawidayat, S., Sargowo, D., Sakti, S. P., & Andarini, S. (2016). The peak of the PQRST and the trajectory path of each cycle of the ECG 12-lead wave. *Indonesian Journal of Electrical Engineering and Computer Science*, 4(1), 169-175.
48. Steinfurt, J., Asbach, S., Odening, K.E., Faber, T.S., Stiller, B., Bode, C. and Biermann, J., (2018). Fascicular parasystole and recurrent syncope—a case report. *European Heart Journal-Case Reports*, 2(1), p.pty020.
49. Swain, H. H., & McCarthy, D. A. (1957). Veratrine, protoveratrine, and andromedotoxin arrhythmias in the isolated dog heart. *Journal of Pharmacology and Experimental Therapeutics*, 121(4), 379-388.
50. Verkerk, A. O., Wilders, R., van Borren, M. M., Peters, R. J., Broekhuis, E., Lam, K., ... & Tan, H. L. (2007). Pacemaker current (I<sub>f</sub>) in the human sinoatrial node. *European heart journal*, 28(20), 2472-2478.

51. Waller, A. D. (1887). A demonstration on man of electromotive changes accompanying the heart's beat. *The Journal of physiology*, 8(5), 229-234.
52. Watanabe, M., Feola, I., Majumder, R., Jangsangthong, W., Teplenin, A. S., Ypey, D. L., ... & Pijnappels, D. A. (2017). Optogenetic manipulation of anatomical re-entry by light-guided generation of a reversible local conduction block. *Cardiovascular Research*, 113(3), 354-366.
53. Weiss, J. N., Nivala, M., Garfinkel, A., & Qu, Z. (2011). Alternans and arrhythmias: from cell to heart. *Circulation research*, 108(1), 98-112.
54. Wengrowski, A. M., Wang, X., Tapa, S., Posnack, N. G., Mendelowitz, D., & Kay, M. W. (2015). Optogenetic release of norepinephrine from cardiac sympathetic neurons alters mechanical and electrical function. *Cardiovascular research*, 105(2), 143-150.
55. Yarlagadda, R. K., Iwai, S., Stein, K. M., Markowitz, S. M., Shah, B. K., Cheung, J. W., ... & Mittal, S. (2005). Reversal of cardiomyopathy in patients with repetitive monomorphic ventricular ectopy originating from the right ventricular outflow tract. *Circulation*, 112(8), 1092-1097.
56. Yuniarti, A.R. and Lim, K.M., (2017). The effect of electrical conductivity of myocardium on cardiac pumping efficacy: a computational study. *Biomedical engineering online*, 16(1), 1-12.